An Investigation of Chemical Landscapes in Aqueous Electrosprays by Tracking Oligomerization of Isoprene

Thesis by

Adair Gallo Junior

In Partial Fulfillment of the Requirements

For the Degree of

Master of Science

King Abdullah University of Science and Technology

Thuwal, Kingdom of Saudi Arabia

November, 2017

EXAMINATION COMMITTEE PAGE

The thesis of Adair Gallo Junior is approved by the examination committee.

Committee Chairperson: Prof. Dr. Himanshu Mishra.
Committee Members: Prof. Dr. Suzana Nunes and Prof. Dr. Luigi Cavallo.

TABLE OF CONTENTS

EXAMINATION COMMITTEE PAGE **2**

LIST OF ILLUSTRATIONS **5**

LIST OF TABLES **9**

ABSTRACT **10**

ACKNOWLEDGEMENTS **11**

Chapter 1: INTRODUCTION **12**

1.1 Aqueous Interfaces 17
1.2 Electrospray Ionization (ESI) 19
1.3 Isoprene 21

Chapter 2: OBJECTIVES **24**

Chapter 3: EXPERIMENTAL SECTION **25**

3.1 Materials 25
3.2 High-speed imaging of electrosprays 25
3.3 Oligomerization of isoprene at gas-liquid and liquid-liquid interfaces 26
3.4 Electrospray Ionization Mass Spectrometry - ESIMS 28
3.5 Proton Nuclear Magnetic Resonance - ^{1}H-NMR 29
3.6 Surface tension 30

Chapter 4: RESULTS **32**

4.1 High-speed imaging of electrosprays 32
4.2 Oligomerization of isoprene 37
4.3 Influence of pH of water on the oligomerization of isoprene at ESI 43
4.4 Proton Nuclear Magnetic Resonance - ^{1}H-NMR 44
4.5 Surface tension 46

Chapter 5: DISCUSSION **48**

5.1 Oligomerization of isoprene under electrospray ionization 48
5.2 Chemical and physical processes in electrosprays 51

Chapter 6: CONCLUSIONS **56**

APPENDICES **58**

REFERENCE LIST **65**

LIST OF ILLUSTRATIONS

Figure 1. 2D schematics of hydrogen bond network for water, hydronium and hydroxyl; Red/blue/yellow correspond to oxygen atoms; White correspond to hydrogen atoms; Lines represent the hydrogen bonds; In blue we have the oxygen of a hydronium ion and in yellow we have the oxygen of a hydroxyl. Notice that the white hydrogen atoms centered with the red oxygen atoms correspond to another plane. 18

Figure 2. 2D schematics of solvation shells around a positive (A) and a negative (B) ion of different sizes; (C) Molecular dynamics of water solvating a sodium ion: note the alignment of the oxygens towards the sodium; Red = oxygen; White = hydrogen; Purple = sodium; Blue = cation; Green = anion; Lines represent the hydrogen bonds. 19

Figure 3. Schematics of a electrospray process; The illustration depicts some possible oxidation reactions at the needle capillary that generate excess positive charges (red) in the solution, which are then repelled from the positive electrode towards the mass spectrometer inlet; Soon after the Taylor cone breaks, the electrospray droplets start to evaporate until they reach an instability limit (Rayleigh), when they start to undergo Coulomb fission. 21

Figure 4. Isoprene molecule (C_5H_8, 2-methyl-1,3-butadiene) and some examples of isoprene oligomers, i.e. terpenes. 22

Figure 5. A summary of the experiments A, B, and C reported in this work along with three possible mechanisms for the oligomerization of isoprene during gas-liquid collisions. (**A**) Liquid-liquid collisions: a 1:6 (v/v) mixture of liquid isoprene and pH-adjusted water was agitated at 1200 rpm (for 6, 60, 360 minutes) followed by ESIMS analysis of the organic phase. (**B**) As-purchased liquid isoprene was injected directly in the ESIMS. (**C**) Gas-liquid collisions: electrosprays of water (pH range 1-13) were collided with a stream of air carrying isoprene gas, followed by mass spectrometric detection (Experimental details in the Methods section). On the right hand side, we present three possible mechanisms for chemical reactions during gas-liquid collisions (Category '**C**'): Mechanism C_1 – as the isoprene molecules adsorb onto the water drop, they react with each other under the influence of high electric fields; Mechanism C_2 - the gas-phase isoprene adsorbs onto the electrically charged water droplets in the electrosprays, which continuously evaporate to become increasingly acidic and catalyze oligomerization; Mechanism C_3 - small clusters of water with an excess proton are ejected during the Coulomb explosions, which protonate isoprene molecules in the gas phase and lead to oligomerization. (Image credits: Ivan Gromicho, KAUST illustrator) 27

Figure 6. Photograph of the experimental setup of ESIMS. 29

Figure 7. Schematic of surface tension measurement via pendant droplet method at NTP; **A**: Air chamber without isoprene; **B**: Air chamber saturated with gaseous isoprene. 31

Figure 8. Photographs of water electrosprayed at positive 6 kV (DC) from a glass needle capillary coated with gold; Needle diameter ~150 μm; The blue arrow represents the flow of positively charged water. 33

Figure 9. Photographs of water electrosprayed at positive 7 kV (DC) applied at a gold wire (diameter of ~100 μm) concentrically to a glass needle capillary coated with a superhydrophobic material (Glaco™); Needle diameter ~150 μm; Arrow legend: glass needle (blue), gold wire (red), observable electrospray zone (green), multiple Taylor cones (orange); The labeling from **a** to **p** does not represent any specific time sequence. 34

Figure 10. High-speed shots of water electrosprayed at positive 7 kV (DC) applied at a gold wire (diameter of ~100 μm) concentrically to a glass needle capillary coated with a hydrophobic material (Glaco™); The pictures are sequenced into time intervals of around 60 μs, except the intervals from **g**-**h** and **h**-**i** which are around 10 μs each. The total time interval from **a** to **j** is 450 μs. From **a** to **c**, we can see the formation of a Taylor cone until it breaks into droplets. In **d**, we start to track (with green arrows) the last droplet formed after the breaking of the Taylor cone; This droplet being of negative charge, is attracted back to the positive electrode (**d**-**g**), until it touches (**g**) the liquid at the capillary tip, then it rapidly gets positively charged, resulting in a Coulomb fission (**h**) and subsequent repulsion form the positive electrode (**i**). 36

Figure 11. ESIMS spectra for sets of experiments A, B, and C: The dominant peaks correspond to protonated oligomers of isoprene, $[(Isop)_n.H]^+$, and the secondary peaks correspond to fragments of the isoprene molecules attached to the primary peaks; (**A**) ESIMS spectra of the organic phase from the emulsion of liquid isoprene in water at pH = 1 (1:6 v/v) that was agitated at 1200 rpm for 360 minutes; (**B**) ESIMS spectra of as-purchased liquid isoprene; (**C**) ESIMS spectra of products of gas-liquid collisions between water (pH = 1) and gas-phase isoprene (Experimental details in the Methods section). 38

Figure 12. ESIMS spectra for gas-liquid collisions, experiments (**C**). (**C1**) Water at p[NaCl] = 5 and flow rate of 1 μL/min; (**C2**) Water at pH = 1 and flow rate of 1 μL/min; (**C3**) Water at pH = 12.3 and flow rate of 1 μL/min; The main peaks correspond to the oligomers of isoprene plus one proton $[(Isop)_n+H]^+$, and are separated by the mass of isoprene (68 *m*/*z*); The four smaller peaks between the main ones correspond to the four possible fragmentations of the carbon bonds within the isoprene molecule (C_5H_8); In all three cases the stream flow of air (600 mL/min) and gaseous isoprene (which evaporated from the air bubbler at ~0.48 g/min) was directed towards the electrosprayed water jet; the temperature of the capillary in the ESIMS was 150 °C, the electrical potential applied at the electrospray needle was 6 kV, the capillary inlet was grounded, and the separation between the needle and the capillary inlet was ~1 cm. 39

Figure 13. Influence of shaking duration on the liquid-liquid collisions, experiments (**A**). Comparison of ESIMS peaks from $(Isop)_2$ (m/z 137 = $2.MW_{ISOPRENE} + MW_{H^+}$) and $(Isop)_6$ (m/z 409 = $6.MW_{ISOPRENE} + MW_{H^+}$); ESIMS set to positive mode, 6 kV, 150

°C, 10 μL/min, pH of aqueous phase 1.52; The shaking time did not considerably influence the signal intensity of the liquid-liquid collisions. 40

Figure 14. Influence of capillary temperature on the detection of $[(M)_n+H]^+$ peaks at the ESIMS. (**B1**) Comparison between signal intensities of peaks from $(Ace)_1$ (m/z 59 = $MW_{ACETONE}$ + MW_{H^+}) and $(Ace)_2$ (m/z 117 = $2.MW_{ACETONE}$ + MW_{H^+}). (**B2**) Comparison of peaks from $(Et)_2$ (m/z 93 = $2.MW_{ETHANOL}$ + MW_{H^+}) and $(Et)_2$ (m/z 138 = $3.MW_{ETHANOL}$ + MW_{H^+}). (**B3**) Comparison of peaks from $(Isop)_1$ (m/z 69 = $1.MW_{ISOPRENE}$ + MW_{H^+}) and $(Isop)_{10}$ (m/z 681 = $10.MW_{ISOPRENE}$ + MW_{H^+}). ESIMS set to positive mode, 6 kV, 10 μL/min for acetone and ethanol, and 5 μL/min for isoprene. The insets in the right corners are characteristic ESIMS spectra for each case. 42

Figure 15. Influence of the ionic strength and ESI voltage on the ESIMS spectra of experimental sets (**A**) and (**C**). On the y-axis, we plot the average mass spectral intensity of all the oligomeric peaks $[(Isop)_n.H]^+$, given by $\Sigma_n I_n/n$, normalized by the highest datum in each plot. (**A**) Liquid-liquid collisions: the ESIMS spectra demonstrated protonation and oligomerization of isoprene after emulsions of isoprene in water with pH ≤ 3.5 and pH > 12 in a 1:6 ratio (v/v) were agitated at 1200 rpm for 360 minutes. (**C**) Gas-liquid collisions: the ESIMS spectra demonstrated protonation and oligomerization of isoprene gas after collision with electrosprays of water with pH ≤ 3.5 and pH > 12, and pH-neutral salty solutions. The sizes of the error bars were similar to or smaller than the symbols used. Curves are added to the plots to aid visualization. 44

Figure 16. (**A**) ^{1}H-NMR spectra of the organic phase after shaking liquid isoprene with pH 1.5 water in a volumetric ratio of 1:6 for 60 minutes. (**B**) ^{1}H-NMR spectra of as-purchased isoprene. (**A1**) ^{1}H-NMR spectra of the condensed exhaust from the electrosprays of the organic phase after the liquid-liquid collision (A) experiments. The nearly identical spectra for experimental sets (A) and (B) demonstrate that there was no detectable (NMR resolution ~ 10 μM) oligomerization of isoprene during the vigorous shaking of emulsions comprised of liquid isoprene with pH 1.5 water in a volumetric ratio of 1:6. 46

Figure 17. Influence of gaseous isoprene on the surface tension of a droplet of water. The surface tension was measured by the pendant drop method in a chamber in the presence of air (blue line) and gaseous isoprene in air (red line). The surface tension of the water droplet changed considerably in the presence of gaseous isoprene, indicating adsorption and possibly dissolution of the isoprene into the bulk water. 47

Figure 18. Simulation of the change in pH during the electrospray process considering only the oxidation reactions R1 and R2. This was based a calculation that considered an electrospray of pH 7 water formed in our ESIMS at a flow rate of 5 μL/min, 8 kV and a constant electric current (DC) of 4.5 μA. 53

Figure 19. Semi-quantitative simulation of the influence of bulk pH and initial droplet radius on the net/excess charge of electrosprayed droplets; For a given ESI setup, the just-formed droplets will have different diameters depending on experimental conditions such as the electric potential, polarity, needle diameter, ionic strength, and surface tension; Assuming a current proportional to the ionic strength of the

solution previous to the ESI; We expect that the sooner the droplets reach the Rayleigh limit, the faster they will undergo Coulomb fissions and release highly reactive clusters containing excess hydronium ions; Let us consider water with pH = 5 (pink line): a droplet of 1000 nm is formed with an excess charge of ~26%, i.e. 10^{-16} C (Point *P*); Since this droplet is below the Rayleigh limit, it will not undergo Coulomb fission immediately. However, this pH 5 droplet will evaporate (following the horizontal arrow) and then, after reaching the Rayleigh limit, undergo Coulomb fission; Note that the down arrow representing fission is exaggerated; it shows a ~10-fold decrease in the droplet charge during each fission, while a lower discharge is expected in reality(109). Conversely, droplets with pH = 1 (black line) would immediately eject hydroniums to the gas phase under same setup conditions. A parallel can be drawn between this process and the proposed Mechanism C_3. Alternatively, the dotted orange line simulates the condition where the current is not proportional to the ionic strength of the solution, i.e. constant current; This was based in a calculation that considered an electrospray of water at initial pH 7 formed in our ESIMS at a flow rate of 5 μL/min, 8 kV and a constant electric current (DC) of 4.5 μA. 54

Figure 20. Semi-quantitative simulation of the influence of bulk pH, initial diameter and electric field on the net/excess charge of electrosprayed droplets. Same assumptions of Figure 19 apply, e.g. current proportional to ionic strength. In this graph, we include the differences that a more pronounced effect of charge separation would cause on the system, causing the just-sprayed droplets to faster reach the Rayleigh limit. 55

LIST OF TABLES

Table 1. Experimental summary 28

ABSTRACT

An Investigation of Chemical Landscapes in

Aqueous Electrosprays by Tracking Oligomerization of Isoprene

Adair Gallo Junior

Electrospray ionization mass spectrometry (ESIMS) is widely used to characterize neutral and ionic species in solvents. Typically, electrical, thermal, and pneumatic potentials are applied to create electrosprays from which charged ionic species are ejected for downstream analysis by mass spectrometry. Most recently, ESIMS has been exploited to investigate ambient proton transfer reactions at air-water interfaces in real time. We assessed the validity of these experiments via complementary laboratory experiments. Specifically, we characterized the products of two reaction scenarios via ESIMS and proton nuclear magnetic resonance (^{1}H-NMR): (i) emulsions of pH-adjusted water and isoprene (C_5H_8) that were mechanically agitated, and (ii) electrosprays of pH-adjusted water that were collided with gas-phase isoprene. Our experiments unambiguously demonstrate that, while isoprene does not oligomerize in emulsions, it does undergo protonation and oligomerization in electrosprays, both with and without pH-adjusted water, confirming that C-C bonds form along myriad high-energy pathways during electrospray ionization. We also compared our experimental results with some quantum mechanics simulations of isoprene molecules interacting with hydronium at different hydration levels (gas versus liquid phase). In agreement with our experiments, the kinetic barriers to protonation and oligomerization of isoprene were inaccessible under ambient conditions. Rather, the gas-phase chemistries during electrospray ionization drove the oligomerization of isoprene. Therefore, we consider that ESIMS could induce artifacts in interfacial reactions. These findings warrant a reassessment of previous reports on tracking chemistries under ambient conditions at liquid-vapor interfaces via ESIMS. Further, we took some high-speed images of electrosprays where it was possible to observe the main characteristics of the phenomena, i.e. Taylor cone, charge separation, and Coulomb fission. Finally, we took the freedom to speculate on possible mechanisms that take place during electrospray ionization that affected our system and possibly may influence other common analytical techniques on ESIMS.

ACKNOWLEDGEMENTS

I thank my mentor, Prof. Himanshu Mishra, for guiding my research and for being a friend. I am grateful to King Abdullah of Saudi Arabia for envisioning this amazing place called KAUST. I am also grateful to an uncountable number of people that impacted positively in my life, especially, Adair, Vera, Carlos, and my friends that shared this space-time with me, Jamilya, Vanessa, Fernanda, Natanael, Gloria, Hamzah, Faisal, Saeed, Lyazzat, Francisco, Tommaso, João, Joel, Ani, and more, my friends from iLab, Andreia, Eddy, Sankara, Patricia, Sreekiran, Ratul, Adriano, etc. I thank you all.

Chapter 1: INTRODUCTION

Interfaces of liquids with solids or gases are two-dimensional regions of molecular thickness(1). Remarkably, the variations in the relative densities across those interfaces could be of the order of 10^{13}/m, which render upon them unique constraints, for instance, hydration of chemical species(2, 3). Further, the molecular environment at interfaces is drastically different from the condensed phase, due to the discontinuity, which renders interfacial molecules somewhat unstable due to lack of bonds(4). Thus, interfaces of liquids could exhibit different physical and chemical properties than bulk liquids.

Our natural world is replete with interfaces of liquids with gases and solids, for instance clouds(5), oceans, soils, plants, and coatings. In fact, interactions between the atmosphere, lithosphere, hydrosphere, and biosphere drive, precipitation, evaporation, and condensation that control climates(6). In biology, interfaces play vital roles in molecular recognition that gives life(7) its directionality, e.g. fusion of vesicles into lipid bilayers(8), activities of membrane-bound enzymes(9), such as ATP-synthase(10). In applied sciences, stable oil-water emulsions are routinely employed in pharmaceutical drugs(11, 12), materials synthesis(13), cosmetics(14), food products(15), and coatings(16, 17). However, despite their ubiquity in natural and industrial realms, a clear understanding of interfacial phenomena at the molecular level is incomplete. For example, the presence and relative abundance of hydronium versus hydroxyl ions, along with other common ions, at the air-water interface have been intensely debated in the chemical physics community(18-23). Similarly, mechanistic insights into the function of

molecular machineries, such as ATP-synthase require a thorough understanding of factors that give rise to proton-fronts at water-lipid interfaces(24). This is due to the fact that direct experimental observations of structure and dynamics at interfaces are excruciatingly difficult. Most recently, due to unprecedented advances in experimental approaches and computational resources, interfacial science of liquids has emerged as the most exciting scientific frontier with multidisciplinary participation.

In this thesis, we investigate chemical and physical properties of interfaces of water under normal temperature and pressure (NTP - 298 K and 1 atm) conditions. More specifically, we are interested in the interfaces of water with hydrophobes, id est, materials that are unable to form hydrogen bonds with water. We differentiate gas-, liquid-, and solid-phase hydrophobes as, (i) Gases: low solubility in water, characterized by Henry's constants, e.g. nitrogen gas(25); (ii) Liquids: immiscibility in water, e.g. hexadecane(26); (iii) Solids: low adhesion at the solid-liquid interface and commonly characterized by high contact angles at the solid-liquid-vapor interface(27), e.g. hydrocarbons, and perfluorocarbons. It is important to realize that the concept of hydrophobicity spans across different states of matter (solid, liquid, and gas) and length scales (e.g. 10^{-9} – 10^{3} m)(28). For instance, at the nanoscale, hydrophobic molecules aggregate as clusters which self-assemble into lipid bilayers and vesicles at higher concentration(8, 24). In contrast, at the macroscale, hydrophobic surfaces are characterized by water-repellency that enables *Namib* beetles(29) and cactus pines(30) to harvest atmospheric fog, water striders to effortlessly skate on water(31), and lotus leaves to stay clean(32), among numerous other examples(33). Hence, a variety of techniques are used to characterize hydrophobicity - for molecular solutes, gas or liquids, one could

exploit an isothermal titration calorimeter(34), for extended solid surfaces force spectroscopy(35) and contact angle goniometry(36) are used. Unfortunately, a multiscale theory of hydrophobic interactions has remained elusive despite decades of experimental and theoretical research(37).

The motivation behind this work was a series of reports on millions-fold accelerations in rates of several chemical reactions at oil-water interfaces, including Diels Alder cycloadditions, e.g. between quadricyclane and dimethyl azodicarboxylate or cyclohexene and bis(trichloroethyl) azodicarboxylate, and Claisen rearrangements, e.g. of naphthyl ether(38, 39). More recently, researchers employed electrospray ionization (ESI) techniques (details in section 1.2) to study chemical reactions at the air-water interface. Zare and co-workers developed microdroplet fusion mass spectrometry and investigated the Pomeranz-Fritsch synthesis of isoquinoline in microdroplets, which contained N-benzylidene-2,2-diethoxyethanamine precursor in water, generated by an ESI process and found a one-million-fold increase in the rates of reactions(40, 41). Cooks and co-workers investigated via mass spectrometry similar accelerations in the rates of a variety of condensed-phase chemical reactions in confined volumes, such as in thin liquid films and Leidenfrost drops(42, 43).

A variety of hypotheses have been presented to explain these accelerations in rate of reactions at water-hydrophobe interfaces, but the underlying mechanisms are still not entirely clear. For instance, Jung and Marcus predicted that the presence of dangling hydrogen bonds at the oil-water interface(18) could stabilize transition states, leading to dramatic rate accelerations(44, 45). Jorgensen and co-workers, on the other hand, refuted that mechanism and postulated that gas-phase hydronium ions at aqueous interfaces

might play a role(19). Beattie argued that the specific adsorption of OH^- ions and faster auto-dissociation of water at water-oil interfaces constituted the underlying mechanism(20-23). However, the most recent report by Beattie and Bonn that demonstrated that the surface tension of nascent drops of water decreases from ~90 mN/m to 72 mN/m within ~1 ms, independent of the pH or ionic strength, casts doubt on the specific adsorption of ions as the sole explanation(46).

To investigate in situ interfacial reactions by mass spectrometry, Colussi and co-workers developed an innovative experimental approach developed based on colliding streams of gases with nebulized sprays of aqueous electrolytes from electrically grounded capillaries, followed by mass spectrometric detection(47-64). The mass spectrometric sampling required application of ~3.5 kV (extractor) potential in the vicinity of the sprays, as previously realized in the secondary electrospray ionization (SESI) mass spectrometry(65-67). Following a related approach, Beauchamp and co-workers investigated products from the ozonation of gas-phase oleic acid at the air-water interface by bubble bursting ionization and interfacial sampling with a piezoelectric acoustic transducer(68). Using this technique, Colussi and co-workers demonstrated that many organic reactions could be performed on the surface of mildly acidic ($pH \leq 3.5$) water, which were thermodynamic inhibited in the condensed phase, including protonation of organic acids, and protonation and oligomerization of isoprene, and other terpenes(57-59). We note that in the condensed phase, those reactions would require superacidic conditions (~50% H_2SO_4)(69). Colussi and co-workers claimed that protons at the air-water interface exhibited “superacidity” that led to dramatic accelerations. They proffered

this mechanism as the basis of atmospheric night cycling of isoprene flux from the biosphere.

In this report, we investigate the oligomerization of isoprene (details in a later section) to elucidate whether the mechanisms for the observed dramatic accelerations in the rates of chemical reactions at air-water and oil-water interfaces are caused by the intrinsic properties of the interface(70), or are shaped by the experimental techniques, such as electrospray ionization and mass spectrometric detection(71). We note that in the case of electrosprays, numerous factors might influence the rates of chemical reactions, including the geometry of the needle, electrical potential, and temperature of the ion source; the separation between the ion sources and the glass capillary inlet; the flow rate and temperature of the sheath gas; the declustering voltage; the evaporation of the solvent; or the detector response(41, 72-75). In fact, it has been debated whether or not ESIMS is capable of sampling species at liquid-vapor interfaces(76, 77), and whether it would shift chemical equilibria(75, 78-80), hence, causing unexpected species to form due to non-equilibrium conditions(40, 79, 81, 82). Therefore, to clarify whether electrosprays are indeed representative of the air-water interface under ambient conditions, we exploited proton nuclear magnetic resonance (^{1}H-NMR) as a complementary, non-invasive probe. For molecular-level insights into our experiments, our collaborators(83) performed quantum mechanical calculations employing density functional theory (M0-6 flavor), which we discuss here.

1.1 Aqueous Interfaces

Water is a special molecule (84-87). The high electronegativity of oxygen atoms in water molecule leads to a charge imbalance within the molecule, which renders a net dipole moment (value 1.8546 D) to the molecule. The free energy associated with hydrogen bonds in bulk water at NTP is $\Delta G = 21$ kJ/mol. In fact, the high surface tension of water, $\gamma_{LV} = 72$ mN/m at NTP is a consequence of the alignment of the water molecules and their hydrogen bonding at the interface in order to reduce their total free energy (Figure 1). The high dipole moment of water allows it to hydrate ions, via ion-dipole interactions (Figure 2). This ability renders water an excellent solvent for polar molecules and salts and also accounts for the auto dissociation of water and stabilization of hydroniums (H_3O^+) and hydroxyls (OH^-) in bulk water at 10^{-7} M (6×10^{16} ions/L) at NTP (Figure 1). Particular interest for the interfacial properties of water has risen in the research community, mainly because of the crucial roles of such interfaces in intracellular biology(84, 85).

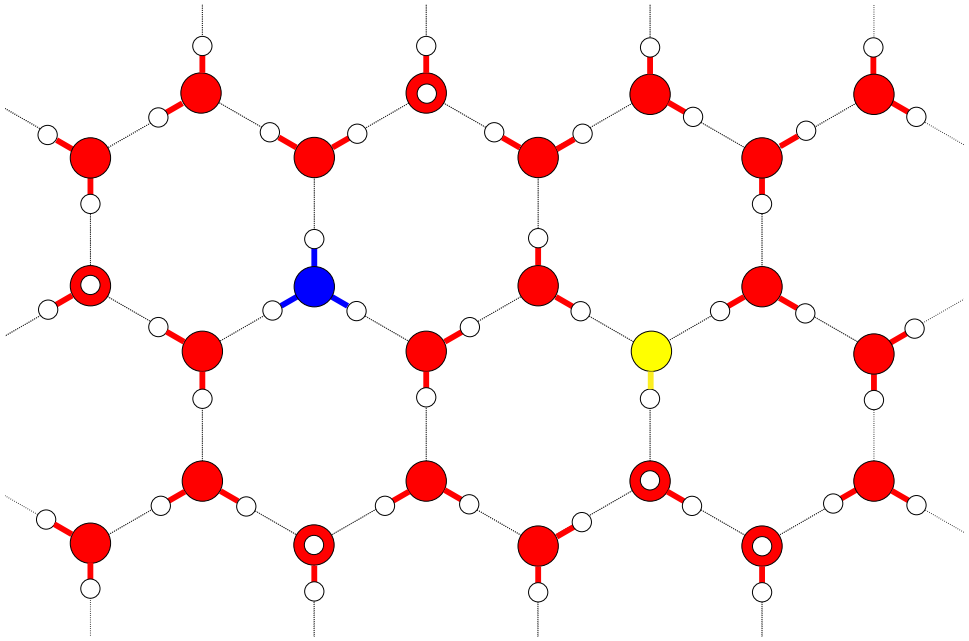

Figure 1. 2D schematics of hydrogen bond network for water, hydronium and hydroxyl; Red/blue/yellow correspond to oxygen atoms; White correspond to hydrogen atoms; Lines represent the hydrogen bonds; In blue we have the oxygen of a hydronium ion and in yellow we have the oxygen of a hydroxyl. Notice that the white hydrogen atoms centered with the red oxygen atoms correspond to another plane.

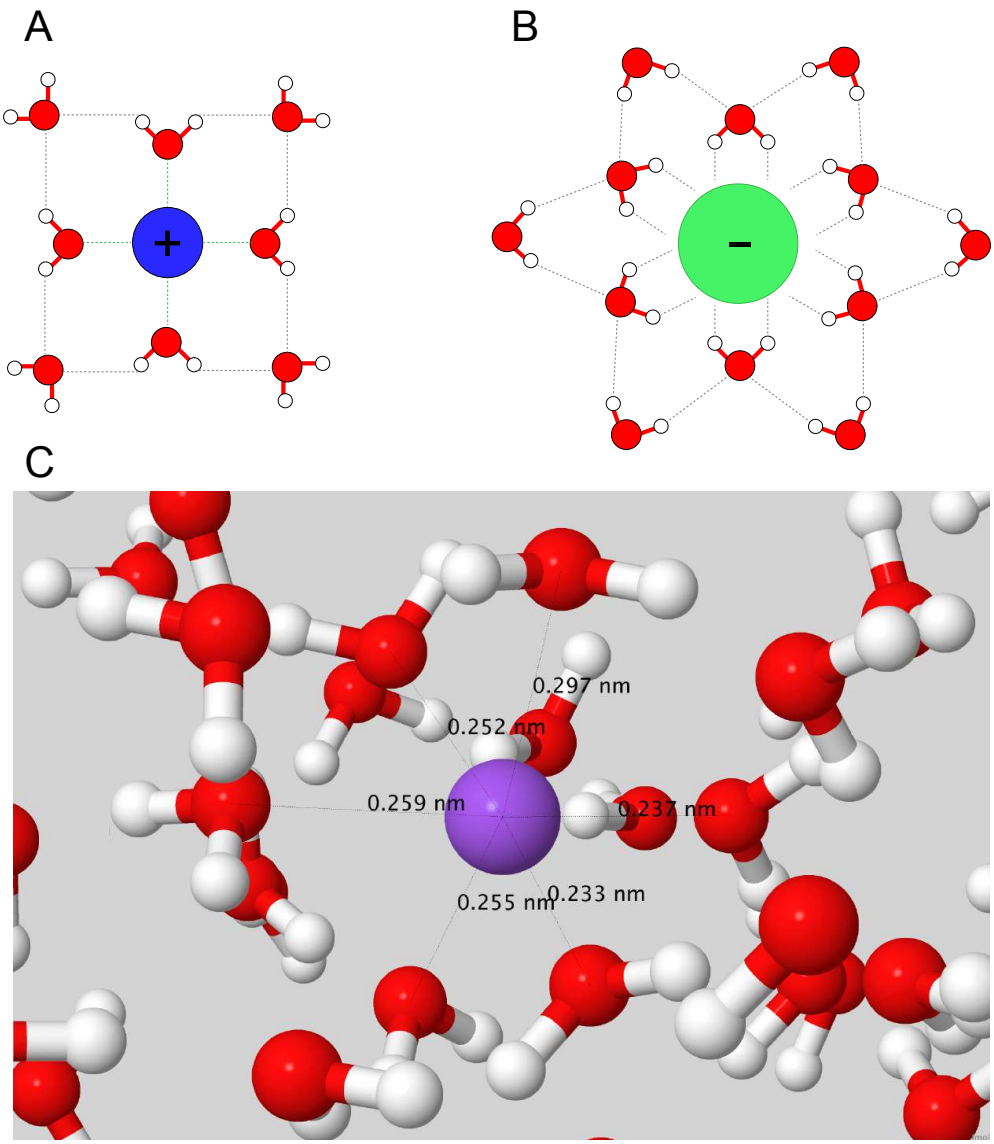

Figure 2. 2D schematics of solvation shells around a positive (A) and a negative (B) ion of different sizes; (C) Molecular dynamics of water solvating a sodium ion: note the alignment of the oxygens towards the sodium; Red = oxygen; White = hydrogen; Purple = sodium; Blue = cation; Green = anion; Lines represent the hydrogen bonds.

1.2 Electrospray Ionization (ESI)

Electrospray ionization mass spectrometry (ESIMS) is a recognized analytical tool across many scientific and engineering disciplines(73-75, 88-90). Usually, the

electrospray ionization (ESI) sources are comprised of a metallic capillary needle kept at a direct current (DC) electrical potential from which solvents containing analytes are passed at rates ~1-100 μL/min. Beyond a threshold voltage, forces driven by electrostatic repulsion of ions overcome the viscous and capillary forces (surface tension) of the liquid, creating Taylor cone jets that eventually break into droplets due to fluid instabilities (Figure 3) (91, 92). These droplets contain excess charges and as the neutral water molecules evaporate the Rayleigh limit is eventually reached, i.e. the repulsion of the electrostatics will overpower the cohesion of the surface tension. The excess charge is predicted to be $Q = (k\pi^2\varepsilon_0\gamma R^3)^{1/2}$, where *d* is the diameter of the droplet at the time of fission, γ is the surface tension of the liquid, ε_0 is the permittivity of a vacuum, and *k* is a constant (73, 92-94). Eventually, ionic species might desorb from neutral solvent molecules via the charge residue mechanism or the ion evaporation model to undergo mass spectrometric detection(74, 75, 90, 95). Despite a significant body of work, some ESI mechanisms are still poorly understood, e.g., electrohydrodynamics of nanojets and tip streaming(91, 92, 96), the ejection of ions from ESI charged droplets(74, 75, 97), and the effects of the electrochemical reactions during the ESIMS process(40, 79).

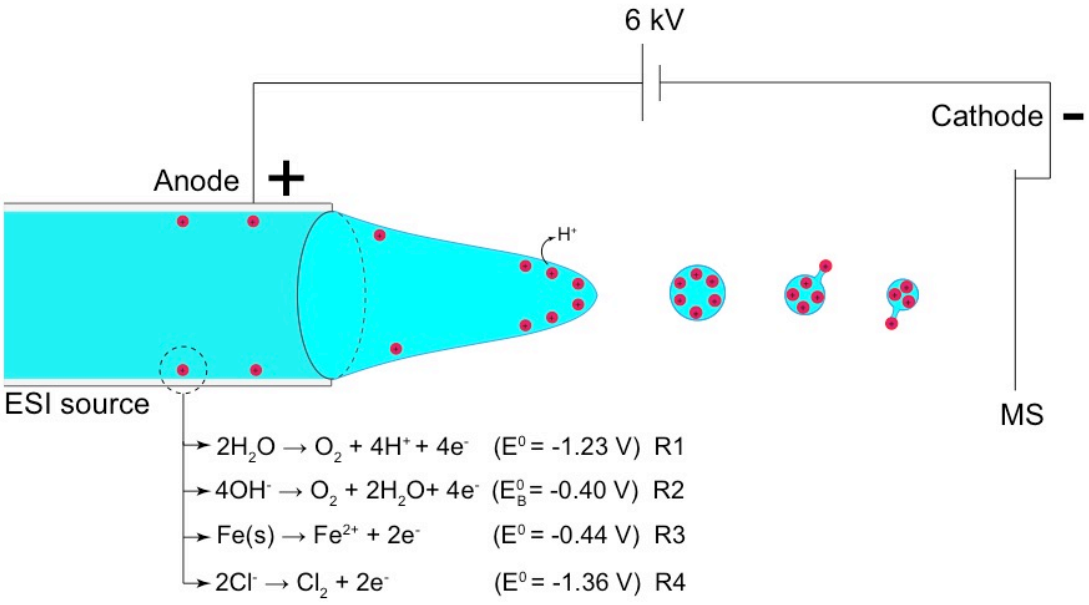

Figure 3. Schematics of a electrospray process; The illustration depicts some possible oxidation reactions at the needle capillary that generate excess positive charges (red) in the solution, which are then repelled from the positive electrode towards the mass spectrometer inlet; Soon after the Taylor cone breaks, the electrospray droplets start to evaporate until they reach an instability limit (Rayleigh), when they start to undergo Coulomb fission.

The generation of excess charges during the electrospray process occurs due to oxidation reactions (when in positive ion mode) at the ESI capillary needle (Figure 3). This is a continuous process and can be quantified by the measured current at the ESI-MS equipment. These reactions can affect the properties of the electrosprayed solution. For instance, in the case of water, an increase in the hydronium concentration can be observed, thus, lowering the pH of the solution.

1.3 Isoprene

Isoprene (C_5H_8, 2-methyl-1,3-butadiene; molecular weight, MW = 68 amu; vapor pressure, p = 61 kPa; boiling point, T_b = 307 K; and solubility in water, S = 0.7 g/L) is

abundant in the atmosphere due to its emission from the biosphere, being one of the most emitted hydrocarbons on the planet. As isoprene gets emitted from the plant leaf, it helps in the thermal regulation of the plant, protecting it from heat. Furthermore, the isoprene base structure can be found in terpenes and isoprenoids, which are important molecules that play critical roles in nature, e.g., carotenes, vitamin A and E, limonene (lemon smell), pinene, etc (Figure 4).

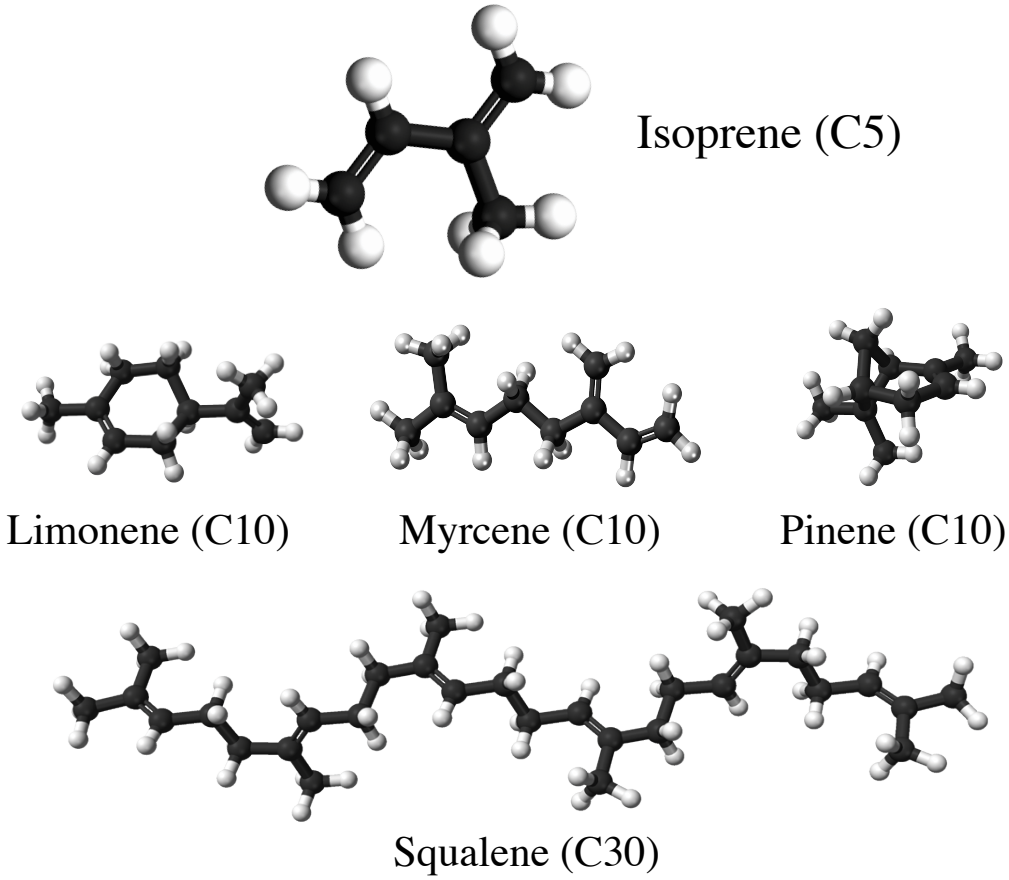

Figure 4. Isoprene molecule (C_5H_8, 2-methyl-l,3-butadiene) and some examples of isoprene oligomers, i.e. terpenes.

An interesting effect involving isoprene has puzzled scientists. During nighttime, the concentrations of isoprene at the canopy of forests decrease rapidly to very low

levels, and it increases again by the next morning when the sun starts to shine, peaking at close to noontime (98-104). This observation is odd because the known mechanisms for the decay of isoprene involve the degradation by short-life hydroxyl radicals, which are naturally produced at the atmosphere by ultraviolet radiation, i.e. during daytime. However, there is still doubt on isoprene's fate at the canopy during nighttime. Some researchers suggested that oligomerization of isoprene to heavier molecules is catalyzed at the interface of dew droplets in the forest, and that it could be the cause for the rapid decay of isoprene during the nighttime, when the lower temperatures facilitate the formation of dew(69). This hypothesis is debunked in this report basically because of the significant differences between droplets formed by condensation or electrosprays (see later sections).

Chapter 2: OBJECTIVES

Based on the points presented in Chapter 1 regarding the controversies about the interfacial properties of water and mechanisms of accelerating chemical reactions on electrosprays and confined volumes, we aimed to provide some experimental insights for the discussion. We used the oligomerization of isoprene in order to understand what were the influences of the main components of the system, i.e. water interfaces, pH/ionic strength, and electrospray ionization source. In summary, we studied the mechanisms of chemical reactions of gas-phase isoprene in electrosprays and compared them with reactions in emulsions of isoprene with pH-adjusted water. Our goal was to answer the following questions that were raised from the previous discussion in Chapter 1:

1. Does the hydrophobicity at the interfaces of water with isoprene provide similar chemical landscape as in the electrosprays?
2. Could we explain the advent of protonation and oligomerization reactions in electrosprays based on the effects of ionic strength and electrochemistries during ESI?
3. Are the oligomerization reactions in electrosprays gas-phase reactions?
4. Finally, is ESIMS a suitable tool to emulate and investigate chemical reactions at ambient air-water interfaces, such as in clouds?

We expect that our experiments and conclusions will shine a light into some inaccurate conclusions previously reached by other researchers.

Chapter 3: EXPERIMENTAL SECTION

We investigated reactions of pH-adjusted water and gas- or liquid-phase isoprene as representative of air-water (vapor-liquid) and oil-water (liquid-liquid) interfaces at normal temperature and pressure (NTP), 293 K and 1 atm(105). We start with electrosprays and then we go into the details of the oligomerization reactions.

3.1 Materials

In our experiments, we used isoprene (99% purity from Sigma-Aldrich), Mili-Q deionized water (18 MΩ-m resistivity), D_2O (99.9% purity from Sigma Aldrich), ethanol (absolute from Merck Millipore), acetone (HPLC standard from VWR Chemicals), NaCl (>99% purity from Sigma Aldrich), HCl (36.9% purity from Fisher Scientific), DCl (35% concentration 99% deuterium purity from Sigma Aldrich), and NaOH (>97% purity from Sigma Aldrich) to adjust the pH and ionic strengths.

3.2 High-speed imaging of electrosprays

We recorded videos of electrosprays using a high-speed camera (Phantom v1212). The setup used to generate the electrosprays was a voltage source (Keithley 2290-10 10kV Power Supply) with the positive electrode connected to (i) a capillary glass needle coated with gold, and (ii) a golden wire inside a capillary glass needle. We used a set of

lenses in order to magnify the image to enable the visualization of a Coulomb fission event.

3.3 Oligomerization of isoprene at gas-liquid and liquid-liquid interfaces

As delineated in Figure 5 and summarized in Table 1, we report on the following three sets of ESIMS and ^{1}H-NMR experiments: (**A**) **Liquid-liquid collisions**: we combined liquid isoprene with either pH-adjusted water or D_2O, $1 \leq pH \leq 13$, in a volumetric ratio 1:6, agitated the emulsions at 1200 rpm in a vortexer at NTP for 6, 60, or 360 minutes, and analyzed the organic phase after phase-separation; (**A1**) **Condensed vapors from electrosprays**: vapors from the atmospheric chamber of the ESIMS (described in experiments **A**) were condensed at 0 °C and analyzed by ^{1}H-NMR; (**B**) **Pure components**: we analyzed pure (as-purchased) isoprene, acetone, and ethanol; (**C**) **Gas-liquid collisions**: we created electrosprays of aqueous solutions with varying ionic strengths and pH, and intersected them with a stream of gas-phase isoprene (0.48 g/min carried by N_2 gas flowing at 600 mL/min, i.e. isoprene gas concentration was 800 mg/L). Hereafter, throughout the paper, we will refer to our experiments on the liquid-liquid collisions as (**A**), condensed vapors from electrosprays as (**A1**), pure isoprene as (**B**), and gas-liquid collisions as (**C**).

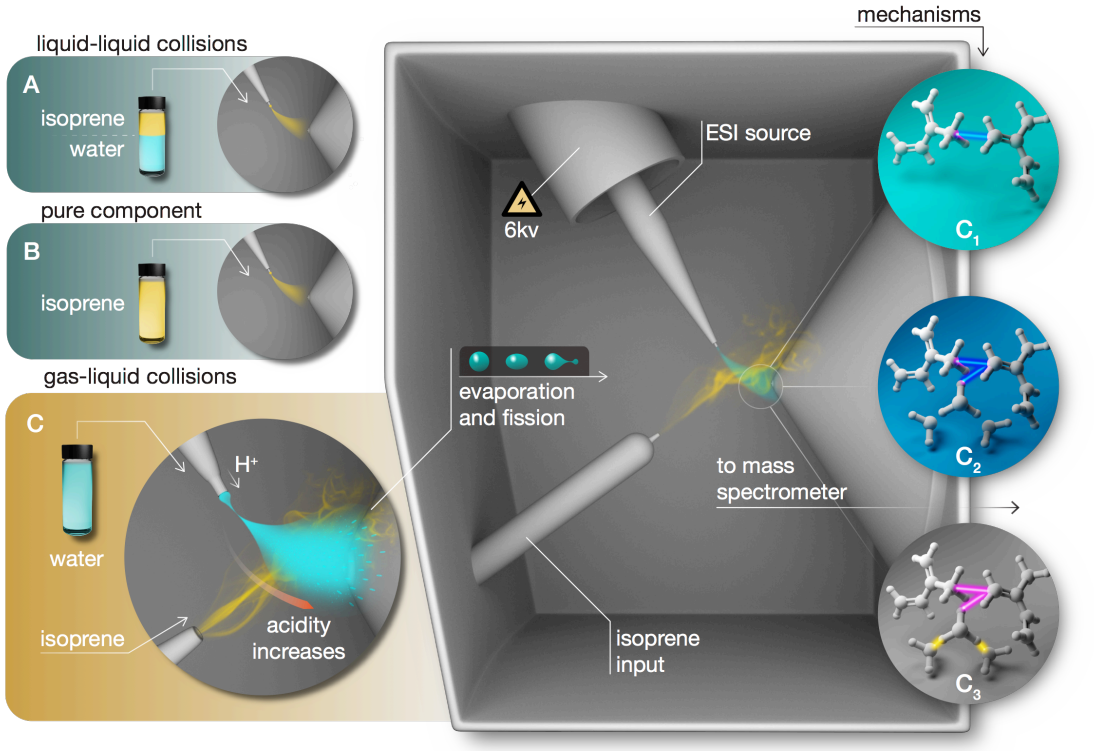

Figure 5. A summary of the experiments A, B, and C reported in this work along with three possible mechanisms for the oligomerization of isoprene during gas-liquid collisions. (**A**) Liquid-liquid collisions: a 1:6 (v/v) mixture of liquid isoprene and pH-adjusted water was agitated at 1200 rpm (for 6, 60, 360 minutes) followed by ESIMS analysis of the organic phase. (**B**) As-purchased liquid isoprene was injected directly in the ESIMS. (**C**) Gas-liquid collisions: electrosprays of water (pH range 1-13) were collided with a stream of air carrying isoprene gas, followed by mass spectrometric detection (Experimental details in the Methods section). On the right hand side, we present three possible mechanisms for chemical reactions during gas-liquid collisions (Category '**C**'): Mechanism C_1 – as the isoprene molecules adsorb onto the water drop, they react with each other under the influence of high electric fields; Mechanism C_2 - the gas-phase isoprene adsorbs onto the electrically charged water droplets in the electrosprays, which continuously evaporate to become increasingly acidic and catalyze oligomerization; Mechanism C_3 - small clusters of water with an excess proton are ejected during the Coulomb explosions, which protonate isoprene molecules in the gas phase and lead to oligomerization. (Image credits: Ivan Gromicho, KAUST illustrator)

Table 1. Experimental summary.

	(**A**) Liquid-liquid collisions	(**B**) Pure components	(**C**) Gas-liquid collisions
	Water(L)-Isoprene(L)	Isoprene(L), Acetone(L), Ethanol(L)	Isoprene(G)-Water(L)
ESIMS	Organics injected	Components injected	Water injected
pH	1-13	-	1-13
pNaCl	-	-	1-7
Shaking time	6, 60, 360 min.	-	-
Voltage	6 kV	6 kV	6-8 kV
Capillary temperature	150 °C	30-330 °C	150 °C
^{1}H-NMR	Organics from (**A**) and condensed vapors (**A1**)	Isoprene(L)	-
pH	1.5	-	-
Shaking time	6, 60, 360 min.	-	-
Aqueous phase	D_2O, H_2O	-	-

3.4 Electrospray Ionization Mass Spectrometry - ESIMS

We performed our experiments in a commercial Thermo Scientific – LCQ Fleet electrospray ionization mass spectrometer in the positive ion mode, where a DC potential of 6-8 kV was applied to the needle, the tube lens voltage was 75 V, the sheath gas flow rate was 10 arb, the pressure was 1.2 torr at the convection gauge and $8x10^{-6}$ torr at the ion-gauge, the flow rates were controlled by a calibrated syringe pump and ranged between 1-10 μL/min, the distance from the ion source and the inlet to the mass spectrometer was ~2 cm, and the distance between the electrospray and the tube ejecting isoprene was 1 cm.

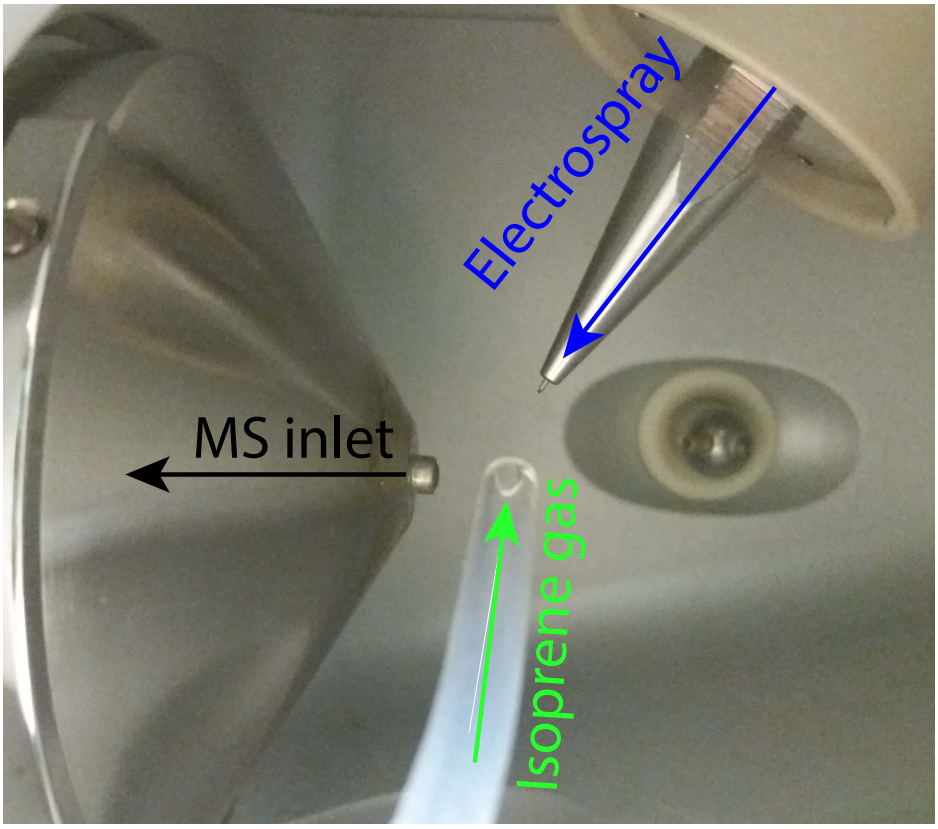

Figure 6. Photograph of the experimental setup of ESIMS.

3.5 Proton Nuclear Magnetic Resonance - ^{1}H-NMR

All NMR spectra were acquired using a Bruker 700 AVANAC III spectrometer equipped with a Bruker CP TCI multinuclear CryoProbe (BrukerBioSpin, Rheinstetten, Germany); Bruker Topspin 2.1 software was used to collect and analyze the data. We transferred 100 µL of the (**A1**) samples into 5 mm NMR tubes, followed by 600 µL of deuterated chloroform ($CDCl_3$). The ^{1}H-NMR spectra were recorded at 298 K by collecting 32 scans with a recycle delay of 5 s, using a standard 1D 90^{o} pulse sequence and standard (zg) program from the Bruker pulse library. The chemical shifts were adjusted using tetramethylsilane (TMS) as an internal chemical shift reference. The (**A**)

samples and a sample of as-purchased isoprene (**B**) were prepared by transferring 100 μL of each to 5 mm NMR tubes, and then adding 550 μL of deuterated water D_2O to the NMR tubes. The ^{1}H-NMR spectra were recorded by collecting 512 scans with a recycle delay time of 5 s, using an excitation sculpting pulse sequence (zgesgp) program from the Bruker pulse library. The chemical shifts were adjusted using 3-Trimethylsilylpropane sulfonic acid (DSS) as an internal chemical shift reference. The free induction decay (FID) data were collected at a spectral width of 16 ppm into 64k data points. The FID signals were amplified by an exponential line-broadening factor of 1 Hz before Fourier transformation.

3.6 Surface tension

The surface tension of water in air was measured in a contact angle cell (Kruss – DSA100E) using the pendant droplet method (calculated with software Kruss – Advance 1.5.1.0) at ambient temperature of 20 °C. This method is based on the deformation of a pendant droplet from a needle, e.g., the higher the surface tension, the more spherical the droplet will be, for a given volume (Figure 7A). We tested the adsorption (and possibly the dissolution) of gaseous isoprene onto the water surface by introducing an opened flask of liquid isoprene into the closed chamber of the angle cell (Figure 7B). Due to its high volatility and low boiling point (34 °C), we expected that vapors of isoprene rapidly reached the saturation levels in the chamber. We alternately saturated and exhausted the chamber (removing all isoprene) in order to get the measurements.

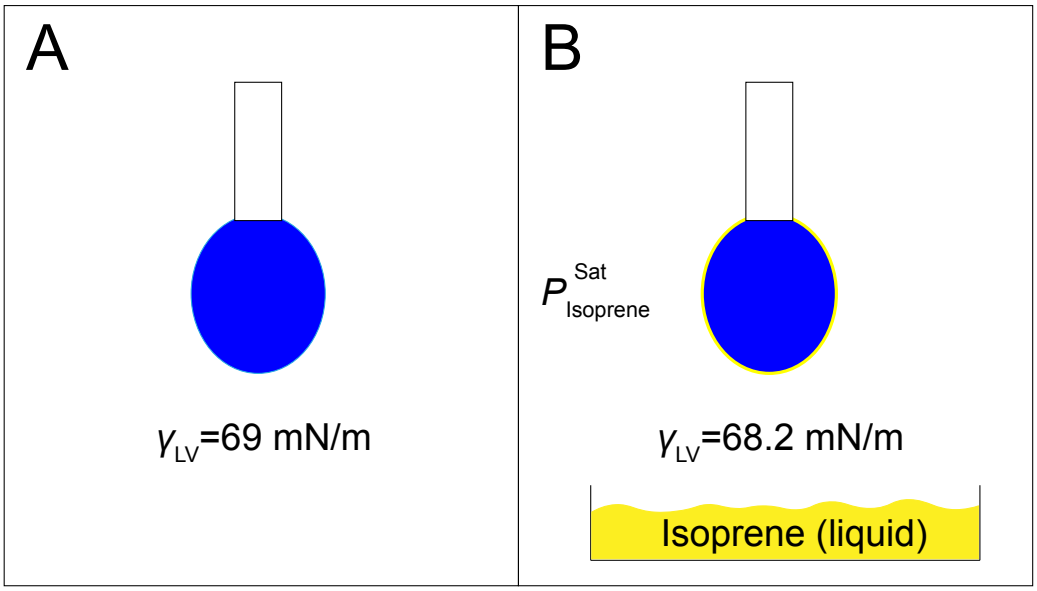

Figure 7. Schematic of surface tension measurement via pendant droplet method at NTP; **A**: Air chamber without isoprene; **B**: Air chamber saturated with gaseous isoprene.

Chapter 4: RESULTS

In this chapter, we first present our results of the imaging of electrosprays in order to give the reader a better understanding on the ESI process itself, and then we go into the details of chemistry of electrosprays and water droplets and the oligomerization of isoprene.

4.1 High-speed imaging of electrosprays

In this section, we present photographs of electrosprays taken with a high-speed camera. The typical electrospray configuration is presented in Figure 8, where we can observe the Taylor cone formation, with an elongated liquid jet that extends until breaking into electrosprayed droplets. It is possible to observe that once the jet breaks into fine droplets, they flow in divergent trajectories due to the same charge electrostatic repulsion. A similar spray is formed in our ESIMS setup, however, the as the diameter of the needle is one order of magnitude smaller, the droplets formed are also smaller, which affect the charging and the evaporation times of those droplets. For instance, it is expected that due to the higher electric field at the smaller needle tip of the ESIMS setup, the droplets depart with a much higher charge density, i.e. they are closer to the instability region, and undergo Coulomb fission at shorter flight times, when compared to the bigger droplets formed at the setup with the gold coated capillary needle.

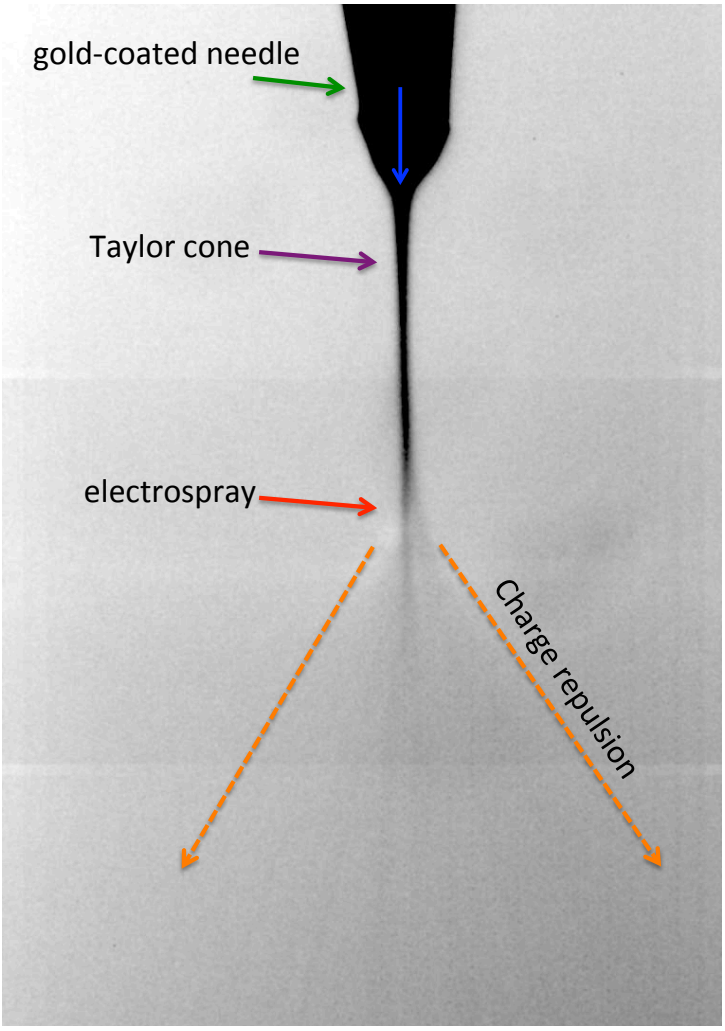

Figure 8. Photographs of water electrosprayed at positive 6 kV (DC) from a glass needle capillary coated with gold; Needle diameter ~150 μm; The blue arrow represents the flow of positively charged water.

Next, in Figure 9 we can see several shots of water being electrosprayed in a slightly different way. Since the electric field is external to the gold wire, the water jets formed are not totally restricted by the needle diameter, thus, allowing for the formation of Taylor cones and electrosprays from bigger liquid droplets. In some cases we can even see multiple Taylor cones formed simultaneously from the same droplet.

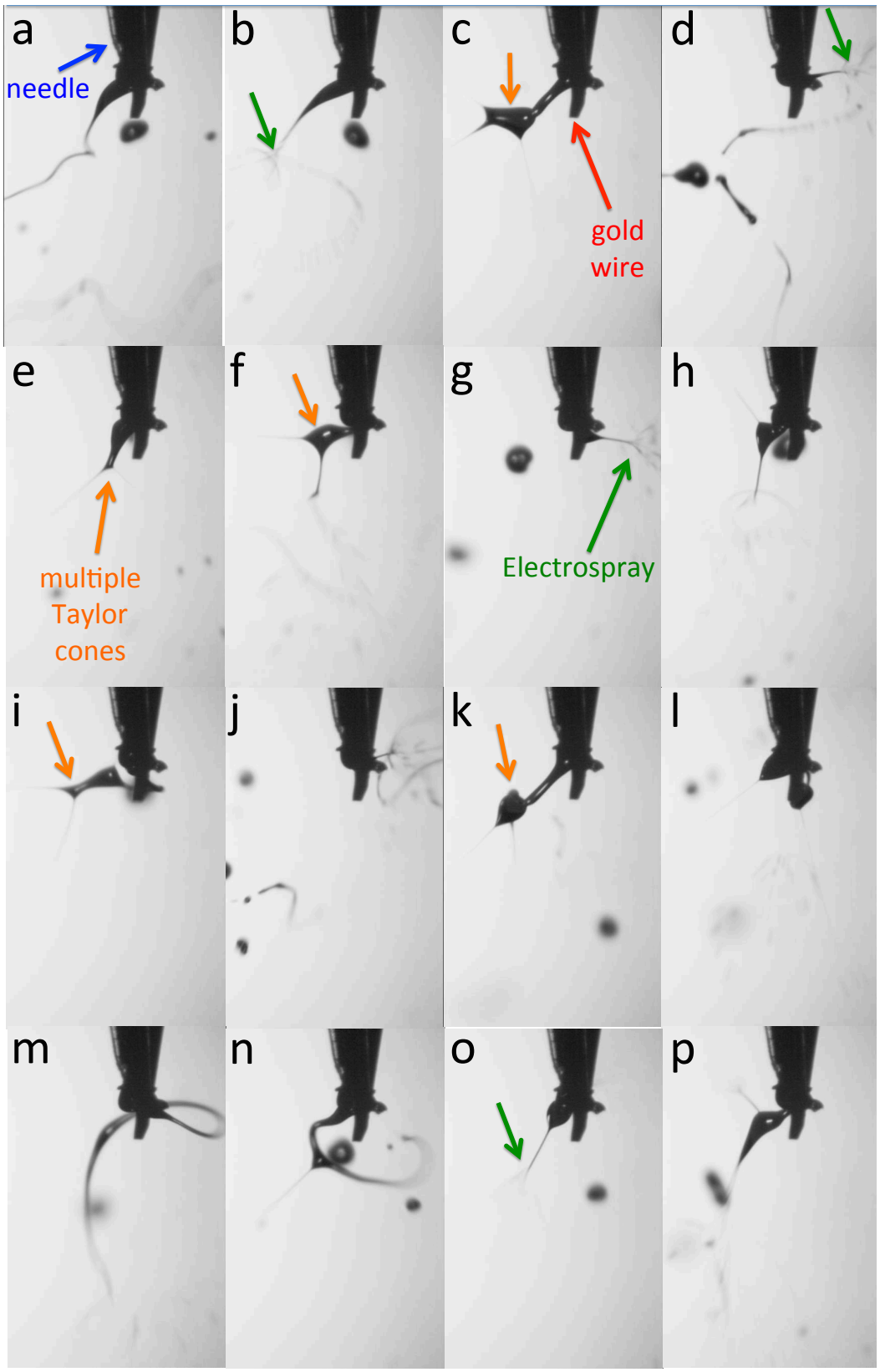

Figure 9. Photographs of water electrosprayed at positive 7 kV (DC) applied at a gold wire (diameter of ~100 μm) concentrically to a glass needle capillary coated with a

superhydrophobic material (Glaco™); Needle diameter ~150 μm; Arrow legend: glass needle (blue), gold wire (red), observable electrospray zone (green), multiple Taylor cones (orange); The labeling from **a** to **p** does not represent any specific time sequence.

In the next sequence of images (Figure 10), we have evidence of the ionic origin of the charges in the electrosprays. We can see the formation of a Taylor cone that separates into a jet (Figure 10**b**), and before this jet breaks into droplets (**c**) the negative ions are attracted towards the part closer to the positive needle. The last droplet (green arrow in **d**) presents a total negative charge, which changes its flight direction by the attractive force towards the positive needle (**d**-**g**). Soon as this droplet touches the liquid in contact with the positive needle (**g**), it releases its negative charges and acquires and excess of positive charges. Promptly, it undergoes Coulomb fission (**h**), due to its small size and high electrical loading (above the Rayleigh limit). And then the droplet is repelled (**i**) without coalescing with the droplet attached to the needle.

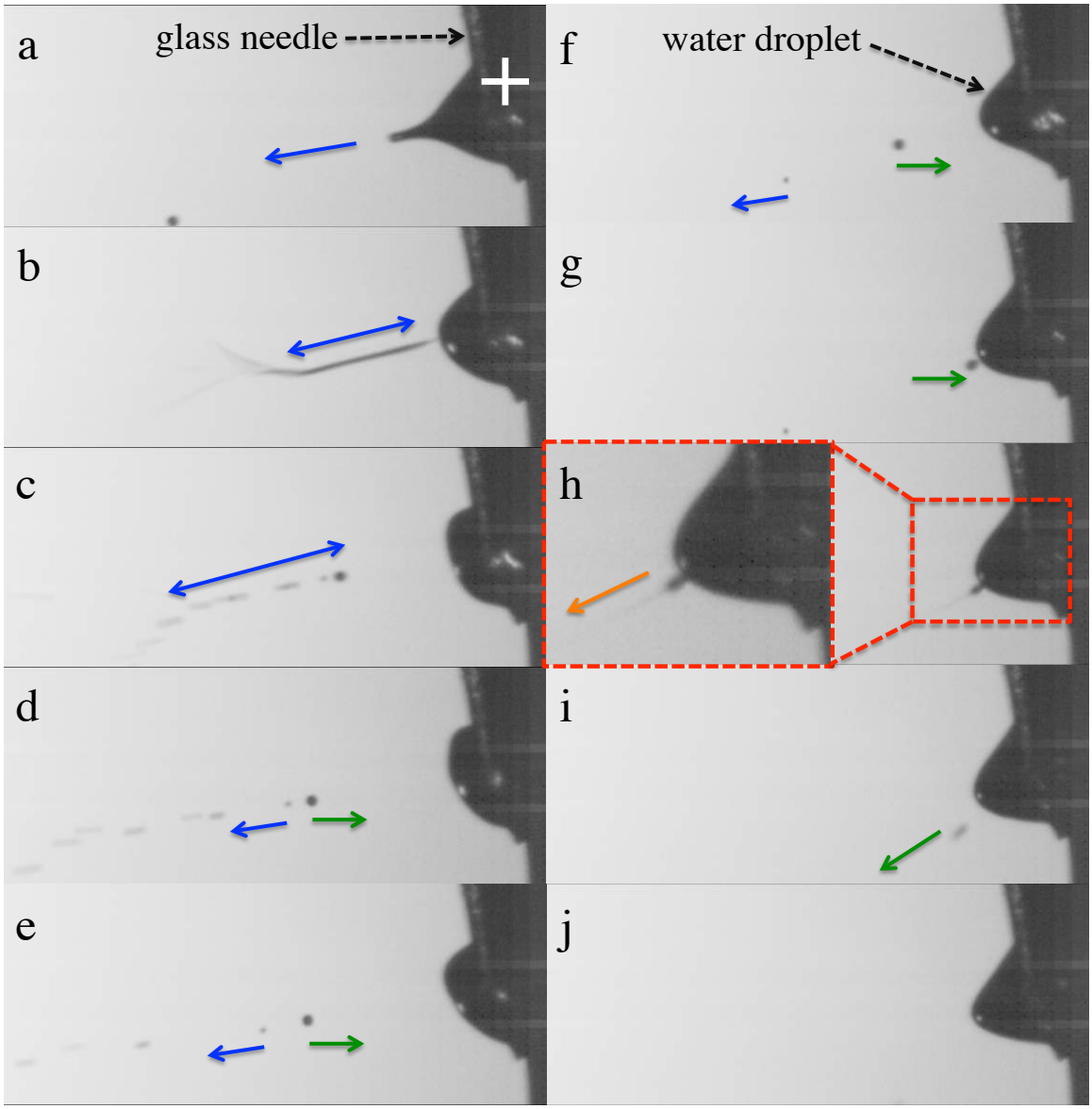

Figure 10. High-speed shots of water electrosprayed at positive 7 kV (DC) applied at a gold wire (diameter of ~100 μm) concentrically to a glass needle capillary coated with a hydrophobic material (Glaco™); The pictures are sequenced into time intervals of around 60 μs, except the intervals from **g**-**h** and **h**-**i** which are around 10 μs each. The total time interval from **a** to **j** is 450 μs. From **a** to **c**, we can see the formation of a Taylor cone until it breaks into droplets. In **d**, we start to track (with green arrows) the last droplet formed after the breaking of the Taylor cone; This droplet being of negative charge, is attracted back to the positive electrode (**d**-**g**), until it touches (**g**) the liquid at the capillary tip, then it rapidly gets positively charged, resulting in a Coulomb fission (**h**) and subsequent repulsion form the positive electrode (**i**).

4.2 Oligomerization of isoprene

In this section and the following ones, we present our results of the experiments proposed in Figure 5 and Table 1. Here, the goal is to understand what are the mechanisms that cause the oligomerization of isoprene at water interfaces, and how different the electrosprayed droplets are from droplets in an emulsion.

The ESIMS spectra from all three sets of experiments (Figure 5) were nearly identical after normalizing with the maximum intensity; see Figure 11A-C for isoprene-water emulsions with pH-adjusted water (**A**), pure isoprene (**B**), and gas-liquid collisions between gas-phase isoprene and pH-adjusted water (**C**) (Figure 12), respectively. The positions of the main peaks in the mass spectra fit the general formula, $[(Isop)_n.H]^+$, which corresponded to covalently bonded oligomers of isoprene with an excess proton (in Figure 14 we present evidence to prove that the peaks did not correspond to physisorbed clusters). We also observed numerous secondary peaks between the primary $[(Isop)_n.H]^+$ peaks that corresponded to the fragmentation of the four carbon bonds in the isoprene molecule (C_5H_8), which formed via myriad possible pathways. While we did not characterize the nature of those species in detail, we speculate that they are composed of isoprene fragments covalently bonded with the $[(Isop)_n.H]^+$ oligomers. In set of experiments (**A)**, we did not see any significant differences among the signal intensities of the ESIMS spectra when the shaking durations were varied from 6 minutes to 60, or even 360 minutes (Figure 13). In the (**C**) experiments, we noticed a peak at m/Z = 233, whose characterization could not be determined (Figure 11C and Figure 12).

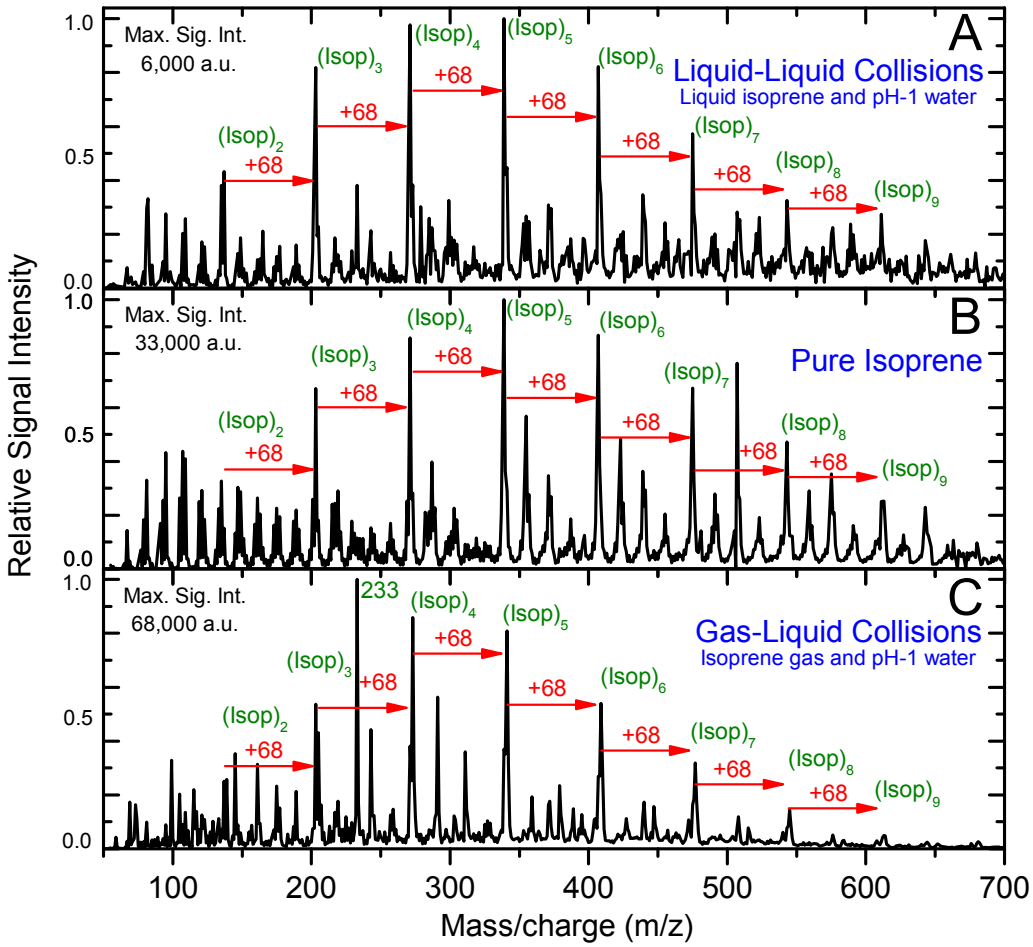

Figure 11. ESIMS spectra for sets of experiments A, B, and C: The dominant peaks correspond to protonated oligomers of isoprene, $[(Isop)_n.H]^+$, and the secondary peaks correspond to fragments of the isoprene molecules attached to the primary peaks; (**A**) ESIMS spectra of the organic phase from the emulsion of liquid isoprene in water at pH = 1 (1:6 v/v) that was agitated at 1200 rpm for 360 minutes; (**B**) ESIMS spectra of as-purchased liquid isoprene; (**C**) ESIMS spectra of products of gas-liquid collisions between water (pH = 1) and gas-phase isoprene (Experimental details in the Methods section).

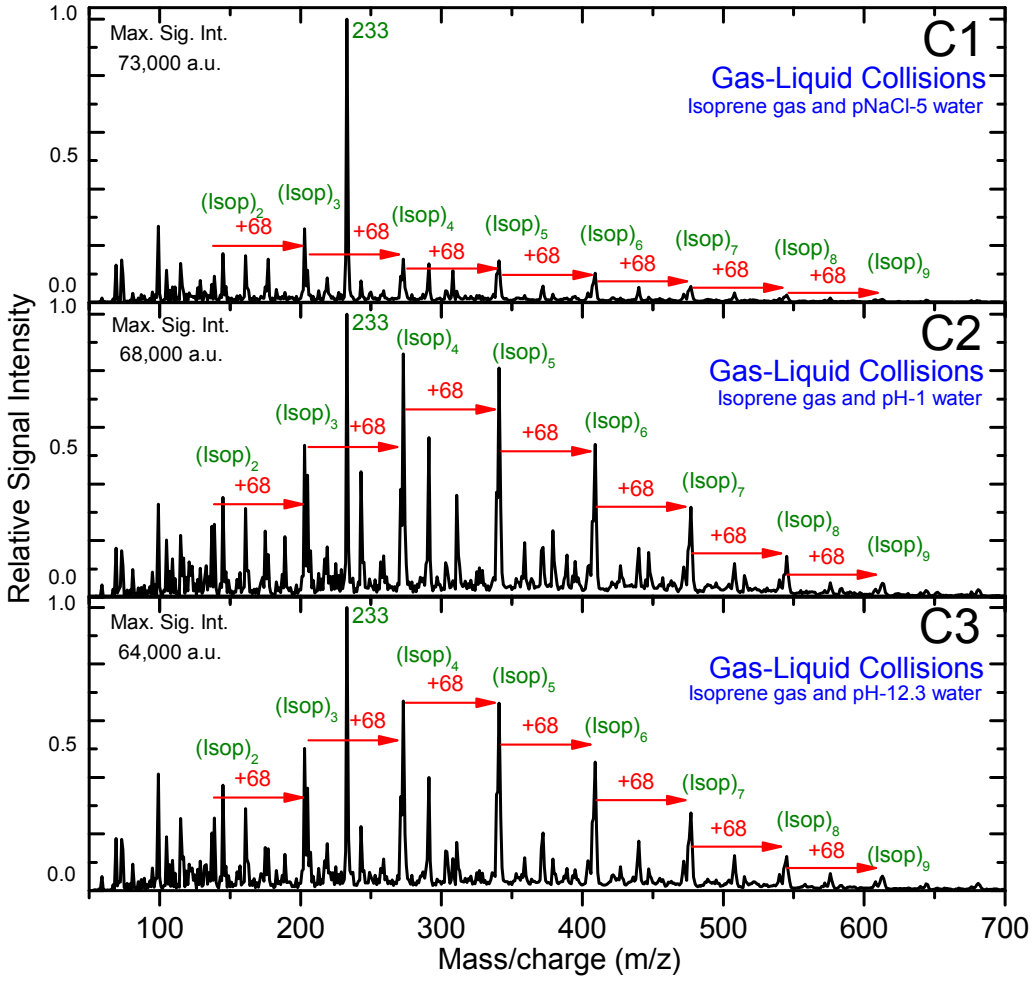

Figure 12. ESIMS spectra for gas-liquid collisions, experiments (**C**). (**C1**) Water at p[NaCl] = 5 and flow rate of 1 μL/min; (**C2**) Water at pH = 1 and flow rate of 1 μL/min; (**C3**) Water at pH = 12.3 and flow rate of 1 μL/min; The main peaks correspond to the oligomers of isoprene plus one proton $[(Isop)_n+H]^+$, and are separated by the mass of isoprene (68 *m/z*); The four smaller peaks between the main ones correspond to the four possible fragmentations of the carbon bonds within the isoprene molecule (C_5H_8); In all three cases the stream flow of air (600 mL/min) and gaseous isoprene (which evaporated from the air bubbler at ~0.48 g/min) was directed towards the electrosprayed water jet; the temperature of the capillary in the ESIMS was 150 °C, the electrical potential applied at the electrospray needle was 6 kV, the capillary inlet was grounded, and the separation between the needle and the capillary inlet was ~1 cm.

The observed signal intensities were surprisingly the stronger in the case of the gas-liquid collisions between *Isop*(g) and acidic water (pH = 1) (**C**), followed by pure isoprene (**B**), and the organic phase from emulsions of liquid isoprene and acidic water

(pH = 1) (**A**). We consider that during the vigorous shaking of the isoprene-water emulsions, a fraction of the aqueous content was dissolved into the organic phase, i.e. isoprene. Subsequently, as the organic phase was electrosprayed after the phase separation, the aqueous components decreased the intensity of the isoprene oligomers due to the competing effect of the ions being attracted into the mass spectrometer. Since our ESIMS has a minimum detection limit of m/z = 50, we were unable to observe those smaller ions. The higher signal intensities (maximum signal intensity 68,000 a.u.) of the gas-liquid collision (**C**) could be attributed to the considerably higher flow rate of isoprene, 0.48 g/min in 600 mL/min of air, into the atmospheric chamber of the ESIMS, compared to 10 μL/min in experiments (**A**) and (**B**).

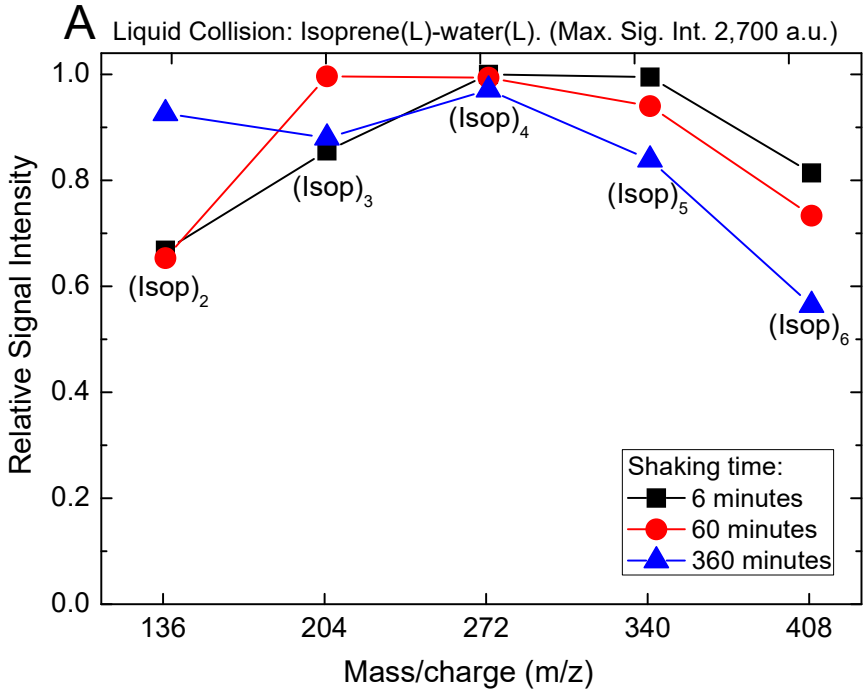

Figure 13. Influence of shaking duration on the liquid-liquid collisions, experiments (**A**). Comparison of ESIMS peaks from $(Isop)_2$ (m/z 137 = $2.MW_{ISOPRENE} + MW_{H}^{+}$) and $(Isop)_6$ (m/z 409 = $6.MW_{ISOPRENE} + MW_{H}^{+}$); ESIMS set to positive mode, 6 kV, 150 °C, 10 μL/min, pH of aqueous phase 1.52; The shaking time did not considerably influence the signal intensity of the liquid-liquid collisions.

The temperature of the glass capillary at the inlet of the mass spectrometer is an important variable in ESIMS. It provides thermal energy to the incoming droplets, facilitating the evaporation of the solvent or neutral molecules – at elevated temperatures, the non-covalently bonded clusters become unstable and the molecules separate, whereas covalently bonded oligomers survive. Thus, based on the changes in the mass spectral intensities as a function of the glass capillary temperature, we could discern if the peaks comprised of covalently bonded or non-covalently bonded species. For instance, while injecting pure acetone, ethanol, and isoprene (Figure 14 – B1, B2, and B3, respectively), we observed peaks in the spectra corresponding to $(M)_n$ ($m/z = n.M + H^+$), i.e., $(Ace)_2$, $(Et)_2$, $(Et)_3$, and $(Isop)_{2,3,4...}$(Figure 14 – top right corner insets). However, as we increased the temperature of the glass capillary, we noticed that the intensities of the heavier peaks of acetone and ethanol dramatically decreased with increasing temperatures (Figure 14 – B1 and B2). In stark contrast, the mass spectral intensities for isoprene did not vary much as the temperature increased (Figure 14 – B3). Thus, our simple experiment helped us conclude that while acetone and ethanol form non-covalent clusters(106) with an excess proton, isoprene forms covalently bonded oligomers. Our conclusion was further corroborated by the clean spectra of acetone and ethanol, evidencing that negligible fragmentation and reactions were present.

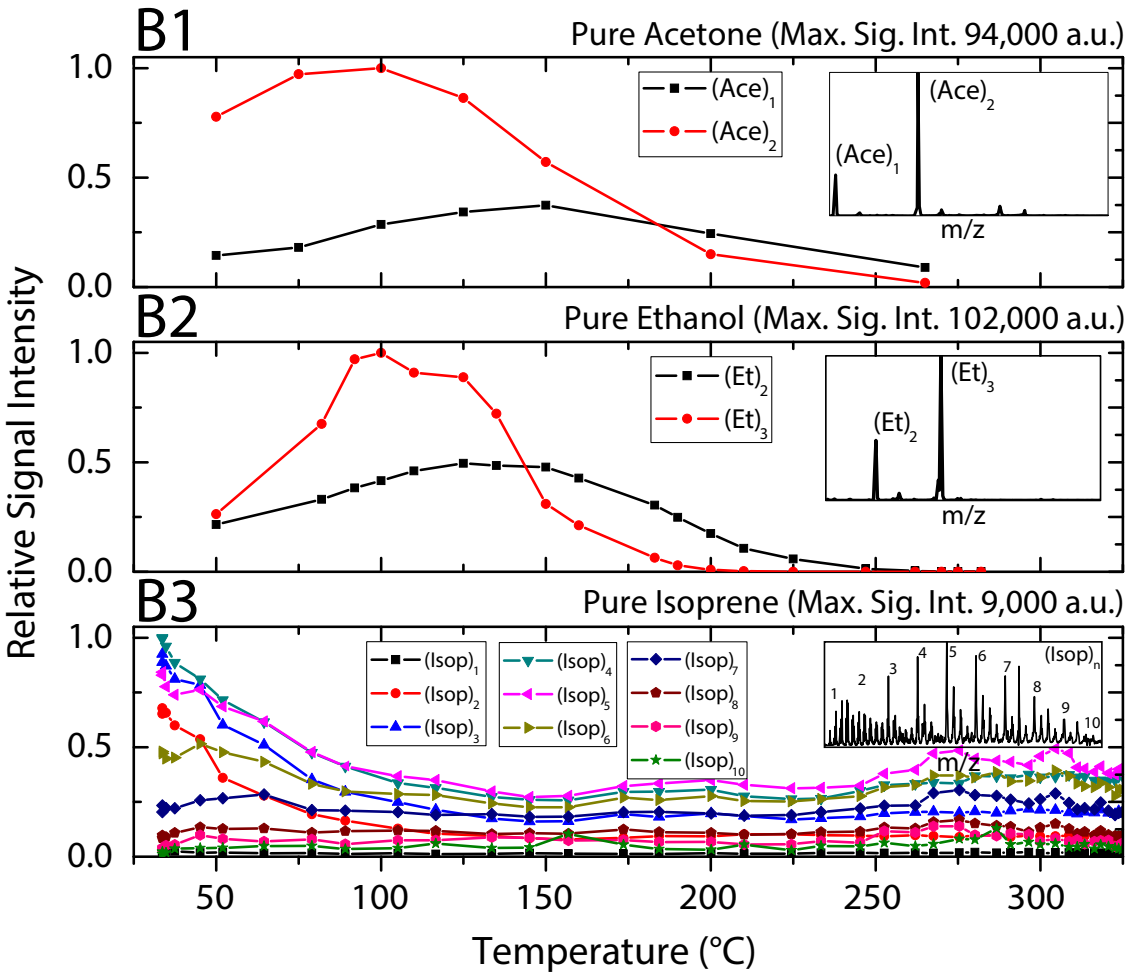

Figure 14. Influence of capillary temperature on the detection of $[(M)_n+H]^+$ peaks at the ESIMS. (**B1**) Comparison between signal intensities of peaks from $(Ace)_1$ (m/z 59 = $MW_{ACETONE} + MW_{H}^{+}$) and $(Ace)_2$ (m/z 117 = $2.MW_{ACETONE} + MW_{H}^{+}$). (**B2**) Comparison of peaks from $(Et)_2$ (m/z 93 = $2.MW_{ETHANOL} + MW_{H}^{+}$) and $(Et)_2$ (m/z 138 = $3.MW_{ETHANOL} + MW_{H}^{+}$). (**B3**) Comparison of peaks from $(Isop)_1$ (m/z 69 = $1.MW_{ISOPRENE} + MW_{H}^{+}$) and $(Isop)_{10}$ (m/z 681 = $10.MW_{ISOPRENE} + MW_{H}^{+}$). ESIMS set to positive mode, 6 kV, 10 µL/min for acetone and ethanol, and 5 µL/min for isoprene. The insets in the right corners are characteristic ESIMS spectra for each case.

4.3 Influence of pH of water on the oligomerization of isoprene at ESI

We investigated the role of pH on the oligomerization of isoprene in our experiments by using emulsions of liquid isoprene and pH-adjusted water in the (**A**) experiments, and collisions between gas-phase isoprene and pH-adjusted water in the (**C**) experiments (Table 1). When examining the products from ESIMS, we noticed that the intensities of the oligomeric peaks $[(Isop)_n.H]^+$ were strongly dependent on the pH of the aqueous phase (Figure 15). These observations have been reported previously and ascribed to the superacidity of water at the air-water interface(57, 59). However, we found that the ESIMS spectra from both experiments, (**A**) and (**C**), presented the same peaks for the acidic, basic, and pH-neutral salty solutions (Figure 15; compare Figure 11 A and C with Figure 12 C1 to C3). Perhaps this is the most important part of this thesis, as we corroborate previous experimental findings(59), but we give a new interpretation to these observations based on different perspectives a new experimental data.

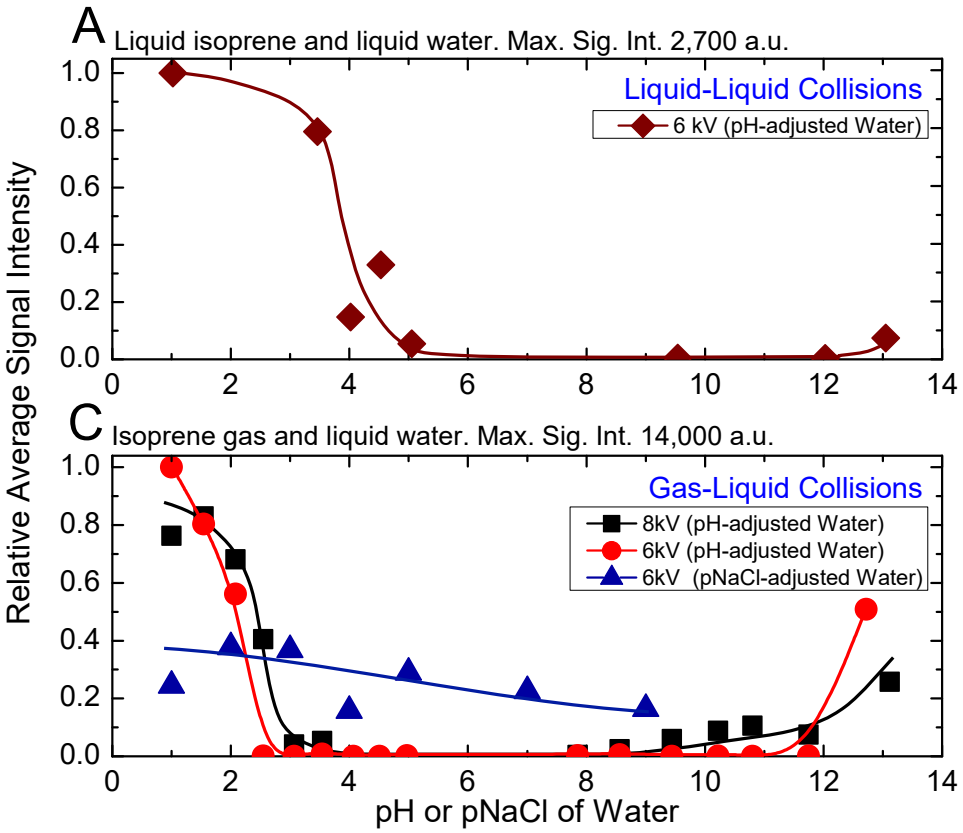

Figure 15. Influence of the ionic strength and ESI voltage on the ESIMS spectra of experimental sets (**A**) and (**C**). On the y-axis, we plot the average mass spectral intensity of all the oligomeric peaks $[(Isop)_n.H]^+$, given by $\Sigma_n I_n/n$, normalized by the highest datum in each plot. (**A**) Liquid-liquid collisions: the ESIMS spectra demonstrated protonation and oligomerization of isoprene after emulsions of isoprene in water with pH ≤ 3.5 and pH > 12 in a 1:6 ratio (v/v) were agitated at 1200 rpm for 360 minutes. (**C**) Gas-liquid collisions: the ESIMS spectra demonstrated protonation and oligomerization of isoprene gas after collision with electrosprays of water with pH ≤ 3.5 and pH > 12, and pH-neutral salty solutions. The sizes of the error bars were similar to or smaller than the symbols used. Curves are added to the plots to aid visualization.

4.4 Proton Nuclear Magnetic Resonance - ^{1}H-NMR

After the emulsions composed of liquid isoprene and water at pH = 1.5 in experimental set (**A**) were vigorously mixed, we waited for phase separation. Then, we compared the organic layers resulting from this phase separation by ^{1}H-NMR as a

function of the mixing time, and by replacing H_2O with D_2O. For completeness, we also recorded the ^{1}H-NMR spectra of pure, as-purchased isoprene (**B**). To our surprise, the ^{1}H-NMR spectra from all of the set (**A**) samples were identical to those of set (**B**), indicating that effects from the duration of shaking (6-360 min), the pH (1-13), and the isotope (H_2O versus D_2O) were all insignificant (Figure 16 A and B). To investigate further, we condensed the vapors from the ESIMS exhaust (**A1**) after injecting the set (**A**) samples ($1 \leq pH \leq 13$), and obtained their ^{1}H-NMR spectra. All of the set (**A1**) samples showed spectra similar to each other (Figure 16 A1). The presence of several new peaks indicated that chemical reactions occurred during the ESIMS (79, 107), mostly leading to fragments of isoprene and oligomers. This is fundamental evidence that the ESI system cannot be assumed to represent a typical water surface, i.e. as found in natural environments.

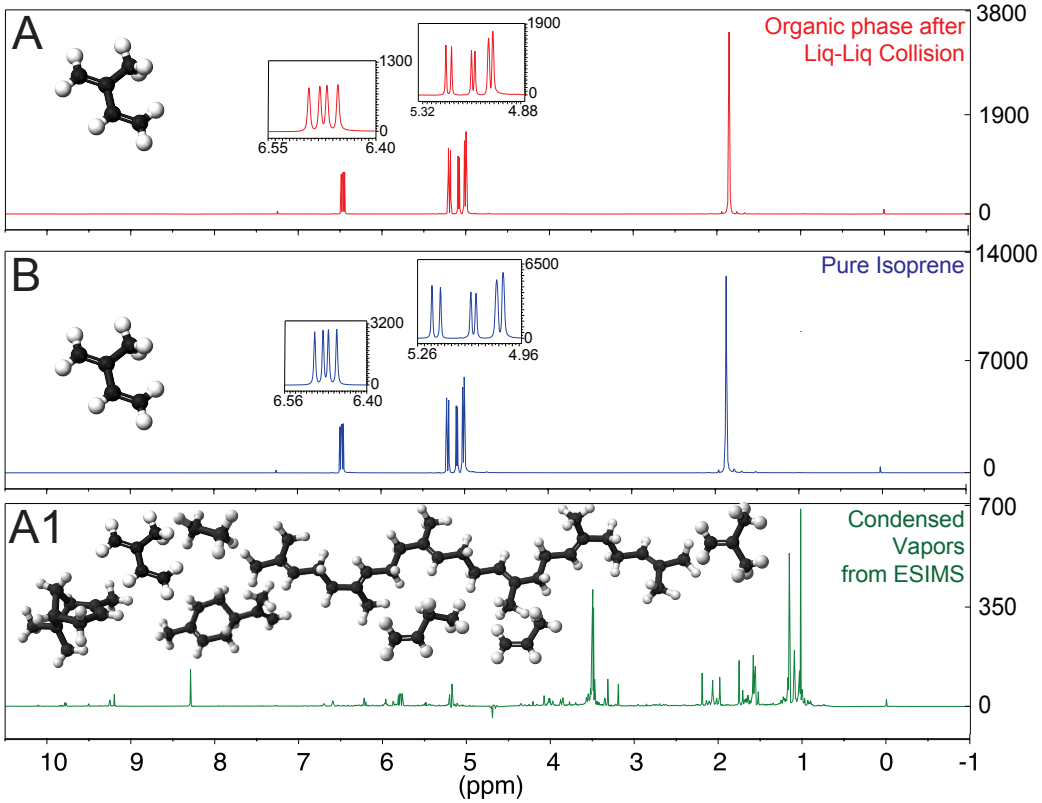

Figure 16. (**A**) ^{1}H-NMR spectra of the organic phase after shaking liquid isoprene with pH 1.5 water in a volumetric ratio of 1:6 for 60 minutes. (**B**) ^{1}H-NMR spectra of as-purchased isoprene. (**A1**) ^{1}H-NMR spectra of the condensed exhaust from the electrosprays of the organic phase after the liquid-liquid collision (A) experiments. The nearly identical spectra for experimental sets (A) and (B) demonstrate that there was no detectable (NMR resolution ~ 10 μM) oligomerization of isoprene during the vigorous shaking of emulsions comprised of liquid isoprene with pH 1.5 water in a volumetric ratio of 1:6.

4.5 Surface tension

We found that, at elevated concentrations, the isoprene molecules adsorbed (and possibly dissolved) onto the water drops under ambient conditions. We demonstrated this by exposing pendant water drops to gaseous isoprene, and measuring the decrease in the surface tension (Figure 17). We expect this to be a similar phenomena, wherein

hydrophobic particles adsorb at the air-water interface to form liquid marbles at a macroscopic scale(108). This effect of isoprene attaching to the droplets could lead to reactions as the conditions of the droplet change during water evaporation.

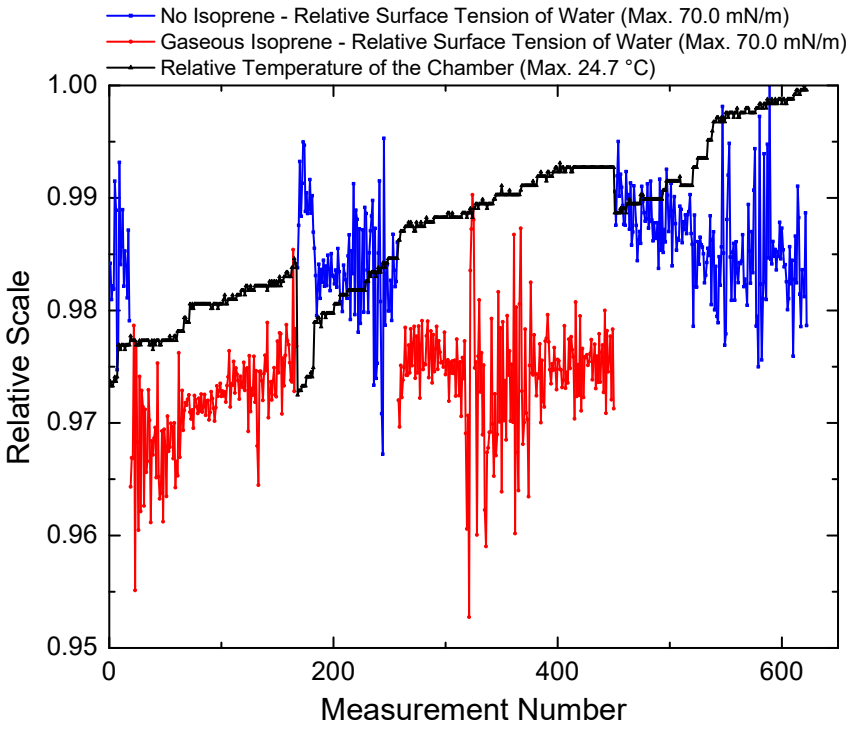

Figure 17. Influence of gaseous isoprene on the surface tension of a droplet of water. The surface tension was measured by the pendant drop method in a chamber in the presence of air (blue line) and gaseous isoprene in air (red line). The surface tension of the water droplet changed considerably in the presence of gaseous isoprene, indicating adsorption and possibly dissolution of the isoprene into the bulk water.

Chapter 5: DISCUSSION

In this chapter, we will start with the analysis of the oligomerization of isoprene under electrospray ionization, following by an in-depth study on the electrospray process itself.

5.1 Oligomerization of isoprene under electrospray ionization

When analyzed via ESIMS, we observed (covalently-bonded) oligomers of isoprene $[(Isop)_n.H]^+$ in all of our experimental sets, (**A**), (**B**), and (**C**) (Figure 11, Figure 12). In set (**A**) experiments, we did not see any significant differences among the signal intensities of the ESIMS spectra when the shaking durations were varied from 6 minutes to 60, or even 360 minutes (Figure 13). Our experiments, (**A**), (**B**), and (**C**), demonstrated that C-C bonds were formed and broken during oligomerization and fragmentation in and on the electrosprays of both acidic and basic water (Figure 15, red circles and black squares, respectively), as well as the pH-neutral saline solutions (Figure 15, blue triangles). The aqueous solutions of higher ionic strengths (acidic, basic, or salty) facilitated fine electrospraying(93, 109). We also observed that, as the voltage used to create the electrosprays was increased from 6 kV to 8 kV, the inflection points shown in Figure 15C shifted such that ionic species were detected at lower ionic strengths.

What are the mechanisms underlying the protonation and oligomerization of isoprene during gas-liquid collisions? As discussed previously, a variety of parameters control the formation of electrosprays, which lead to the mass spectrometric detection of

ions(40, 41, 72-75, 79, 81, 95, 110-113). For our gas-collision system, we consider that the chemical activity, a_i, of species i, (e.g. H_3O^+ or isoprene) at the air-water interface depends on the species' concentration, C_i, the electrical potential, ΔV, and the extent of hydration, given by $a_i = e^{-\mu_i/RT}$, where $\mu_i = \left((\mu_i^c)_{Hydr} + \mu_i^e\right) = \left(RT \times \ln(C_i)_{Hydr} + q\Delta V\right)$. Thus, based on our experimental observations, we propose three key mechanisms (Figure 5):

Mechanism C_1 – the gas-phase isoprene molecules (partial pressure in our chamber: 0.28 atm) adsorb and get concentrated onto the water droplets, proceeding with oligomerization under the influence of high electric fields and higher concentrations of isoprene (adsorbed), i.e. higher activities;

Mechanism C_2 – similarly to the previous mechanism, the gas-phase isoprene adsorbs onto the electrically charged water droplets (with excess protons)(114) in the electrosprays, which continuously evaporate to become increasingly acidic and catalyze oligomerization; or

Mechanism C_3 – small clusters of water (at super acid conditions, i.e. hydroniums), with an excess proton, are ejected during the Coulomb explosions, which could protonate isoprene molecules in the gas phase and lead to oligomerization (Details in a later section). Mechanism C_3 is similar to that of proton transfer reaction mass spectrometry (PTRMS), which has been exploited to detect trace gases in the atmosphere(115).

For all of the above-mentioned mechanisms, the initial pH or salt concentration of water was crucial to the formation of a stable stream of charged water droplets(75, 93, 95, 109). In fact, due to the charge separation under the influence of high electric fields, electrosprayed droplets carry a net charge (109, 110). Hence, it is expected that the electrosprayed droplets are more acidic (or more positively charged with other cations) than the bulk water in the syringe at the moment of water droplet-jet separation(109, 110). It is also possible that the characteristics of the counter-ions are also important for the formation of stable electrosprays. Intriguingly, for pH-adjusted water, we detected oligomers (Figure 15C) when pH ≤ 3.5 or pH > 12 (at 6 kV); whereas for the NaCl solutions, we observed oligomers at concentrations as low as 10^{-9} M. Obviously, the more acidic or basic the initial state of the droplets, the higher the extent of the charge separation under electric fields and the faster they approach the Rayleigh limit on evaporation, at which point the electrostatic self-energy ($kQ^2/\varepsilon\varepsilon_o R$) exceeds the interfacial energy ($4\pi R^2\gamma_{LV}$), where Q is the net charge on the drop, R is its radius, k is a constant, ε is the relative dielectric constant for the medium in comparison to that of air, and γ_{LV} is the surface tension of water (Figure 19, Figure 20)(94). Furthermore, the higher intensities of the oligomers in water having a pH ≤ 3.5 in comparison to the salty solutions indicate that mechanisms C_2 and C_3 are possibly dominant (Figure 15 C).

To further corroborate our experimental results, we recall the theoretical insights into the protonation and oligomerization of isoprene on a molecular scale during the ESI processes given by Mishra et al.(83), where they carried out quantum mechanics calculations (density functional theory) on simple model systems of water molecule clusters with an excess proton (Details in APPENDIX A - Figure A 1 to Figure A 5).

While working with a cluster of 36 water molecules and an excess proton, $(H_2O)_{35}{\cdot}H_3O^+$, to represent the air-water interface, they found the kinetic barriers to protonation of isoprene to be $\Delta G^{\ddagger}$ = 25.5 kcal-mol^{-1}, and the barrier to oligomerization, $\Delta G^{\ddagger}$ = 40.2 kcal-mol^{-1} (APPENDIX A – Figure A 1). These kinetic barriers could not be surmounted within 1 ms under normal temperature and pressure conditions, as evidenced by our ^{1}H-NMR results (Figure 16 A and B). To simulate chemical reactions of isoprene in our electrosprays along mechanism C_3, we investigated the interactions of a smaller cluster, $(H_2O)_3.H^+$, with an isoprene molecule. We found that they readily formed an adduct with the release of ΔH^0 = - 14.2 kcal-mol^{-1} and ΔS^0 = - 43.7 cal-K^{-1}-mol^{-1} from the loss of the translational and rotational degrees of freedom (APPENDIX A – Figure A 1). The subsequent proton transfer was impeded by an easily surmountable barrier of $\Delta G^{\ddagger}$ = 5.8 kcal-mol^{-1} barrier, consistent with our ESIMS experiments. Further oligomerization with an additional isoprene molecule was impeded by a barrier of $\Delta G^{\ddagger}$ = 2.1 kcal mol^{-1} (APPENDIX A – Figure A 2). Thus, these simple models provide qualitative insights into the mechanisms of proton transfers during the ESIMS processes, which are otherwise kinetically hindered on extended interfaces of mildly acidic water with hydrophobes.

5.2 Chemical and physical processes in electrosprays

How do electrochemical reactions at the ESI needle affect the ion concentration in the electrosprayed droplets? Oxidation reactions occur at the ESI needle generating an excess of positive charges in solution (Figure 3). These excess

charges (i.e. H^+ for our system) will be repelled from the ESI needle, forming the electrospray jet. The oxidation reactions can follow either reactions R1 or R2, depending on the concentration of hydroxyl ions available in solution. For instance, at 8 kV and flow rate of 5 μL/min, our ESIMS was giving an electric current (DC) of 4.5 μA. This means that it was generating an excess of charges in solution at a rate of 4.5×10^{-6} C-s^{-1}. Thus, it adds and excess of 5.59×10^{-4} mol/L of H^+, or removing the same amount of OH^-, or a combination of both processes (Figure 18). For this calculation we did not consider other relevant sources of electrons, the most obvious one being the oxidation of ESI needle itself (R3, and other similar reactions forming iron oxides or hydroxides) or oxidation of other ions present for adjusting the pH (R4, for instance). At a constant electric current of 4.5 μA, the needle would oxidize iron at a rate of 0.1 mg/day following only R3. This oxidation is the most favorable, considering the oxidation potentials of the reactions (R1, R2, R3 and R4).

$$2H_2O \rightarrow O_2 + 4H^+ + 4\,e^- \;\;|\;\; E_0 = -1.23\,V \qquad \text{(R1)}$$

$$4OH^- \rightarrow O_2 + 2\,H_2O + 4\,e^- \;\;|\;\; E_0 = -0.40\,V \qquad \text{(R2)}$$

$$Fe(s) \rightarrow Fe^{2+} + 2\,e^- \;\;|\;\; E_0 = +0.44\,V \qquad \text{(R3)}$$

$$2Cl^- \rightarrow Cl_2 + 2\,e^- \;\;|\;\; E_0 = -1.36\,V \qquad \text{(R4)}$$

However, the potential at the ESI needle is much higher, characterizing an overpotential that could drive all the abovementioned reactions. Thus, we expect the oxidation of the most abundant component in the system, i.e. water (Reaction R1). It is important to clarify that even though our simulations are based on the experimental data, we still lack some information in order to be certain about the dominant processes involved. We will perform those experiments in the near future. We speculate that we can

use the electrical current data to estimate the oxidation rates at the needle tip. Thus, by varying the solution composition, we will be able to estimate the how each component facilitates the oxidation reactions and the creation of excess charges for the electrospray. This discussion has the purpose of bringing to the attention of the reader the fact that there is a production of excess charges at the ESI needle, and that sometimes the ions generated can have an effect on the analyte and in the solution.

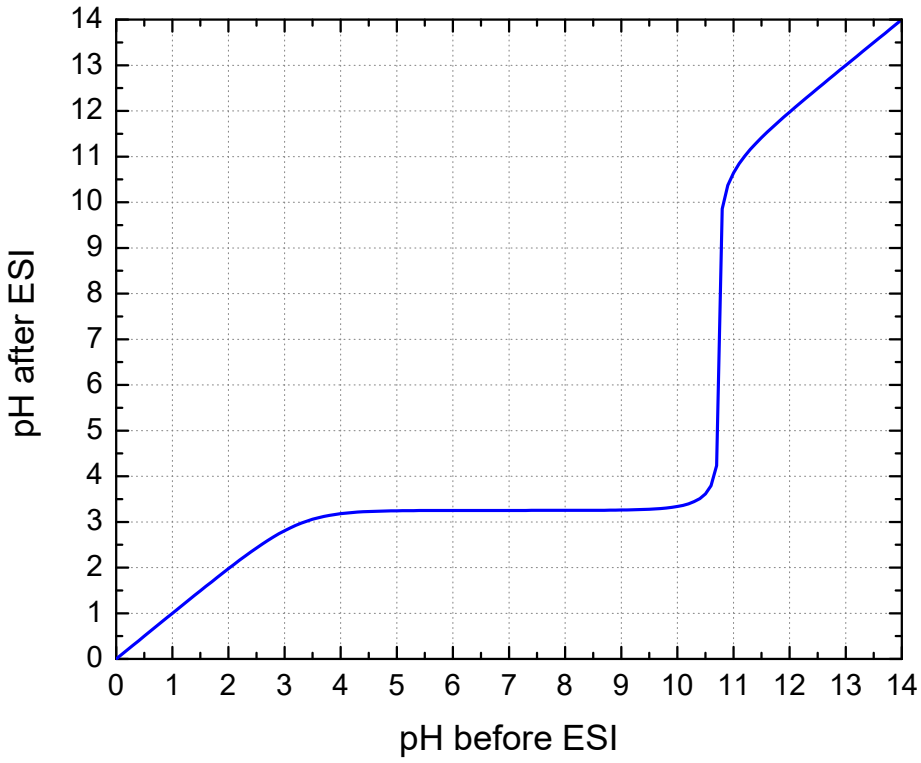

Figure 18. Simulation of the change in pH during the electrospray process considering only the oxidation reactions R1 and R2. This was based a calculation that considered an electrospray of pH 7 water formed in our ESIMS at a flow rate of 5 μL/min, 8 kV and a constant electric current (DC) of 4.5 μA.

What is the role of the net positive charge during droplet formation at the electrospray? Let us consider that the charge separation (and oxidation reactions) at the metallic needle ejecting an analyte under electric fields leads to a decrease in the pH of

the just-formed droplets by at least 0.1 (or a 26% increase in the concentration of protons)(109, 110). In other words, we are assuming that the oxidation reactions at the capillary will generate an excess of protons proportionally to the proton concentration in solution previously to the ESI. It is important to mention that for this scenario the electric current would be proportional to the ionic strength. The initial droplet size will depend on the electric potential, polarity, needle diameter, ionic strength, surface tension, and viscosity (Figure 19 and Figure 20 contain a semi-quantitative representation of this thought experiment). While evaporating, the charge density of the droplets increases and the Rayleigh limit is eventually reached.

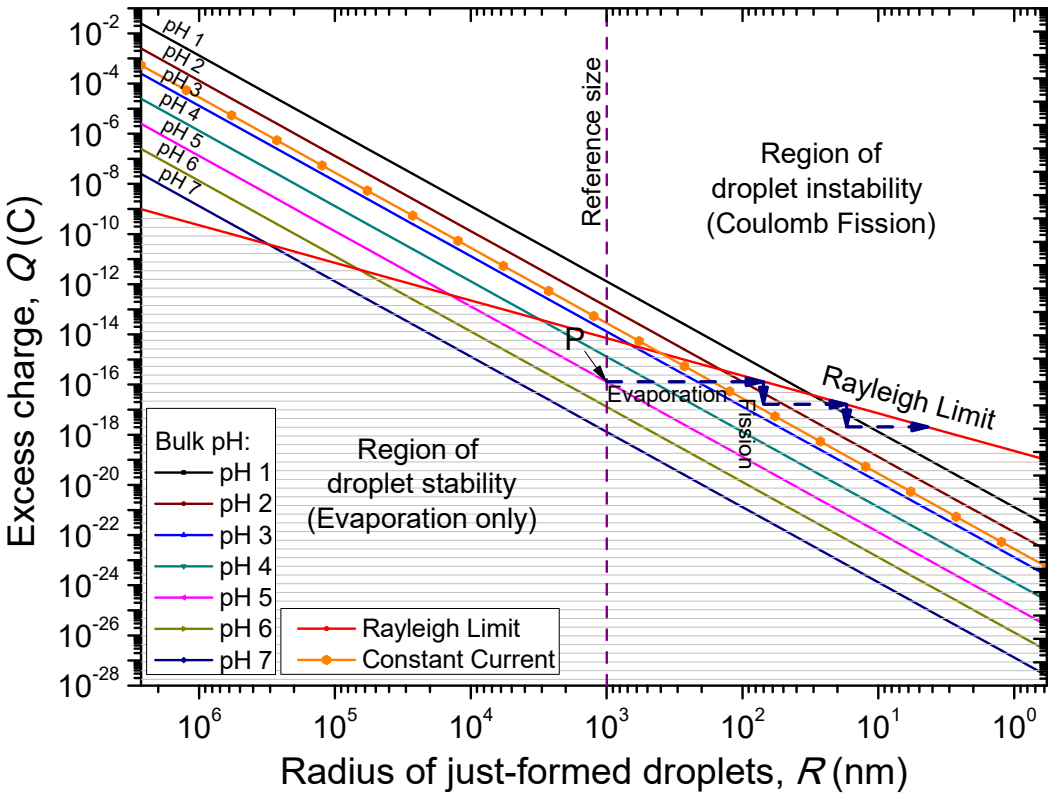

Figure 19. Semi-quantitative simulation of the influence of bulk pH and initial droplet radius on the net/excess charge of electrosprayed droplets; For a given ESI setup, the just-formed droplets will have different diameters depending on experimental conditions such as the electric potential, polarity, needle diameter, ionic strength, and surface

tension; Assuming a current proportional to the ionic strength of the solution previous to the ESI; We expect that the sooner the droplets reach the Rayleigh limit, the faster they will undergo Coulomb fissions and release highly reactive clusters containing excess hydronium ions; Let us consider water with pH = 5 (pink line): a droplet of 1000 nm is formed with an excess charge of ~26%, i.e. 10^{-16} C (Point *P*); Since this droplet is below the Rayleigh limit, it will not undergo Coulomb fission immediately. However, this pH 5 droplet will evaporate (following the horizontal arrow) and then, after reaching the Rayleigh limit, undergo Coulomb fission; Note that the down arrow representing fission is exaggerated; it shows a ~10-fold decrease in the droplet charge during each fission, while a lower discharge is expected in reality(109). Conversely, droplets with pH = 1 (black line) would immediately eject hydroniums to the gas phase under same setup conditions. A parallel can be drawn between this process and the proposed Mechanism C_3. Alternatively, the dotted orange line simulates the condition where the current is not proportional to the ionic strength of the solution, i.e. constant current; This was based in a calculation that considered an electrospray of water at initial pH 7 formed in our ESIMS at a flow rate of 5 μL/min, 8 kV and a constant electric current (DC) of 4.5 μA.

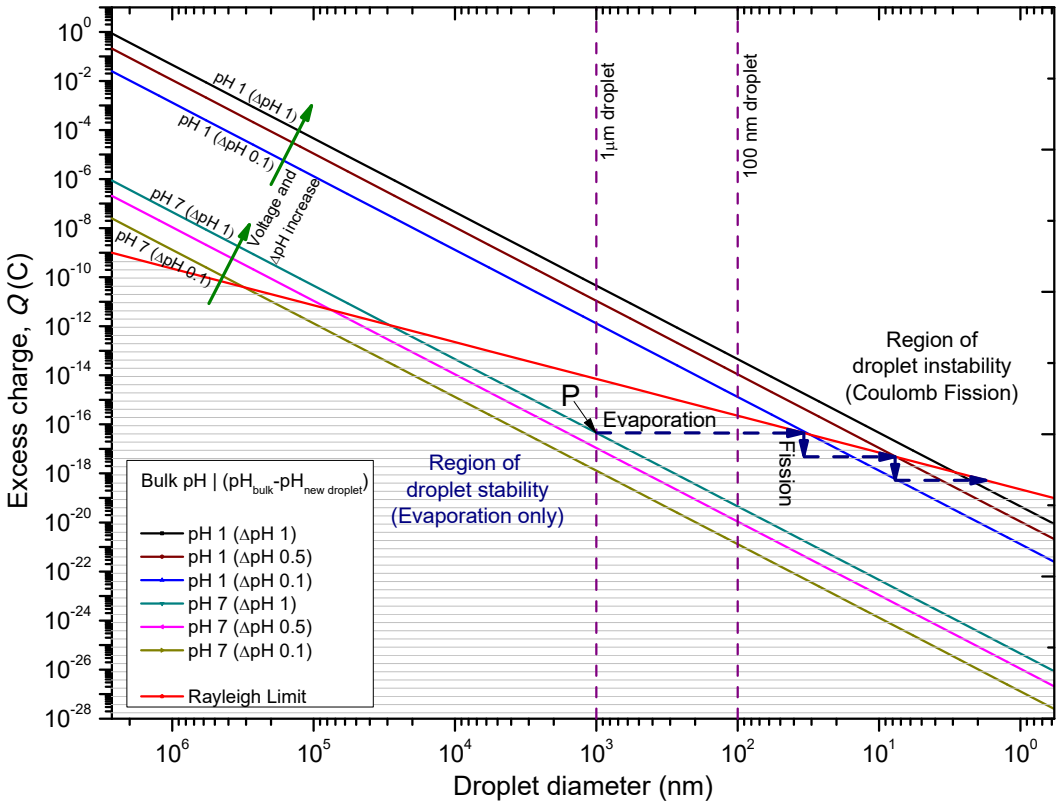

Figure 20. Semi-quantitative simulation of the influence of bulk pH, initial diameter and electric field on the net/excess charge of electrosprayed droplets. Same assumptions of Figure 19 apply, e.g. current proportional to ionic strength. In this graph, we include the differences that a more pronounced effect of charge separation would cause on the system, causing the just-sprayed droplets to faster reach the Rayleigh limit.

Chapter 6: CONCLUSIONS

The value of ESIMS as a tool for quantifying species in solutions is unquestionable due to its high sensitivity and unambiguous output. Similarly, its potential applications in unraveling the physical and chemical phenomena at the air-water interfaces could be highly beneficial, for example, in understanding the heterogeneous chemistries in the atmosphere. However, these potential applications call for an in-depth investigation to establish whether or not ESIMS alters the physical and chemical processes at the air-water interface, especially when the reactant approaches from the gas-phase. In this regard, our experimental and theoretical results demonstrate that ESIMS can induce unexpected reactions. In the case of liquid-liquid collisions of isoprene with mildly acidic water for up to 6 hours, we found no evidence of oligomerization via ^{1}H-NMR. However, when the organic phase (isoprene) was investigated via ESIMS, we found signals of $[(Isop)_n.H]^+$, irrespective of it being shaken with acidic, basic, or salty water. Thus, our results cast doubts on the capability of ESIMS to report on interfacial chemistries at air-water interfaces in real time. Also, other researchers have suggested that charge accumulation on micro- or nanoscale droplets (diameter, 1 μm < d < 15 μm) and extreme evaporation rates were crucial for observing dramatic rate accelerations in microdroplets(40-42, 76, 77, 80, 81). Thus, recent ESIMS reports on the superacidity of protons at extended air-water interfaces under ambient conditions at pH ≤ 3.5 might warrant a reinterpretation. We also suggest that the scope of the ‘on-water’ oligomerization of atmospheric isoprene on mildly acidic environmental surfaces might be minimal. We end by noting that, if the chemical species are chosen

such that they do not participate in the gas-phase or redox chemistries in electrosprays, then it might be possible to investigate liquid-vapor interfaces via ESIMS. When reactants are present in the liquid phase, thin films(116) and Leidenfrost drops(113) might also present unbiased platforms to harness interfacial effects towards expediting chemical reactions.

In-depth investigations, especially with complementary techniques and theoretical predictions, are needed pinpoint factors underlying dramatic rate accelerations in those systems. Our future work will be on gathering experimental data to better understand the effects of the ionic strength of the solution before the formation of the electrospray. In other words, we aim to understand which of the previous graphs (Figure 18, Figure 19 and Figure 20) better describes the ESI process. We expect to be able to correlate the ionic strength and composition of the solution with the electric current generated and with the oxidation reactions taking place at the ESI needle (anode in the positive mode ESI). This will be of great relevance, because we will be able to correctly adjust the data on Figure 19. Thus, it will be possible to predict the whether the electrosprayed droplets will instantaneously undergo Coulomb fission processes or whether they will need to release some of the neutral water molecules under evaporation until reaching the instability region. Consequently, it may be possible to estimate the amount of hydronium ions formed in the gas phase during the short time between the electrospray needle and the MS inlet, region in which the gas collision happens, and possibly understand which of the proposed mechanisms is responsible for the oligomerization reactions.

APPENDICES

Appendix A. Computational Simulation of the System Isoprene(G)-hydronium(G/L)

Here are presented some quantum mechanics calculations performed by our collaborators(71, 83) that corroborate our experiments results with theoretical simulations. They carried out density functional theory (DFT) calculations at the M06 level to provide an accurate description of the ground-state thermochemistry and thermochemical kinetics of the isoprene (*Isop*) and water clusters(117-120). The calculated transition state structures and energies of a series of organic reactions with M06 are in good agreement with the experimental data(119). Researchers have evaluated the binding energies of water clusters, $(H_2O)_n$ (range n = 2-8, 20), as well as the hydration and neutralization energies of hydroxide and hydronium ions using DFT functionals (M06, M06-2X, M06-L, B3LYP, X3LYP), and compared these energies against high-level theory (CCSD(T)/aug-cc-p VDZ level)(117). They found the results from M06 to be in excellent agreement with the high-level theory, both with and without the basis set superposition error correction. Then they carried out single-point electronic energy, E_{elec}, including the diffuse 6-311G**++ basis-set for all atoms(121). The Hessians at these geometries were calculated to determine that the minima and transition states led to 0 and 1 imaginary frequency, respectively. The transition state structures were obtained by following the steep ascent or descent along the vibration mode with one imaginary frequency until the saddle point was reached. The vibrational frequencies from the Hessians were also used to provide the zero-point energies and vibrational contributions

to the enthalpies and entropies. The free energies of isoprene at 1 atm were calculated using statistical mechanics for ideal gases. Under their experimental conditions (and ours as well), the ions were separated by distances larger than the sizes of their clusters, so they excluded counter-ions from the calculations.

Their initial predictions of the proton transfer thermodynamics between H_3O^+(g) and *Isop*(g) were ΔG^0 = -30.7 kcal mol^{-1}, in accordance with the experimental gas-phase basicities (GB) of H_2O (GB_{H2O} = -157.7 kcal mol^{-1}) and *Isop* (GB_{ISO} = -190.6 kcal mol^{-1}), ΔGB = -32.9 kcal mol^{-1}(Figure A 3)(122). Furthermore, the trans- or cis-Isop(g) spontaneously adds to (Isop.H^+ + H_2O), leading to cyclic (ΔG^0 = - 40 kcal mol^{-1}) or acyclic monoterpenes (ΔG^0 = - 9 kcal mol^{-1}) (Figure A 4 and Figure A 5), as noted by other researchers(69, 123). They simulated small clusters of water with an excess proton produced during the ESIMS processes as $(H_2O)_3.H^+$. Since the proton was insufficiently hydrated in this cluster, it exhibited extreme acidity. The incipient isoprene molecule (*ISOP*) fell into a shallow potential well forming an adduct (Figure A 2). The free energy barrier for proton transfer from $(H_2O)_3.H^+$ to *ISOP*(g) was $\Delta G^{\ddagger}$ = 6.9 kcal mol^{-1}; the barrier to subsequent oligomerization with another free ISOP(g) was $\Delta G^{\ddagger}$ = 2.1 kcal mol^{-1}. As shown in Figure 5 of the manuscript, the kinetic barriers for protonation and oligomerization of isoprene on a larger $(H_2O)_{35}.H^+$ cluster were $\Delta G^{\ddagger}$ = 25.5 kcal mol^{-1} and $\Delta G^{\ddagger}$ = 40.2 kcal mol^{-1}, respectively, which are insurmountable under ambient conditions within a 1 ms time frame. Thus, their models are representative of the high-energy ESIMS processes, which can generate hydronium ions, relatively free of water molecules, and consequently, corroborate the hypothesis of gas-phase reactions (mechanism C_3).

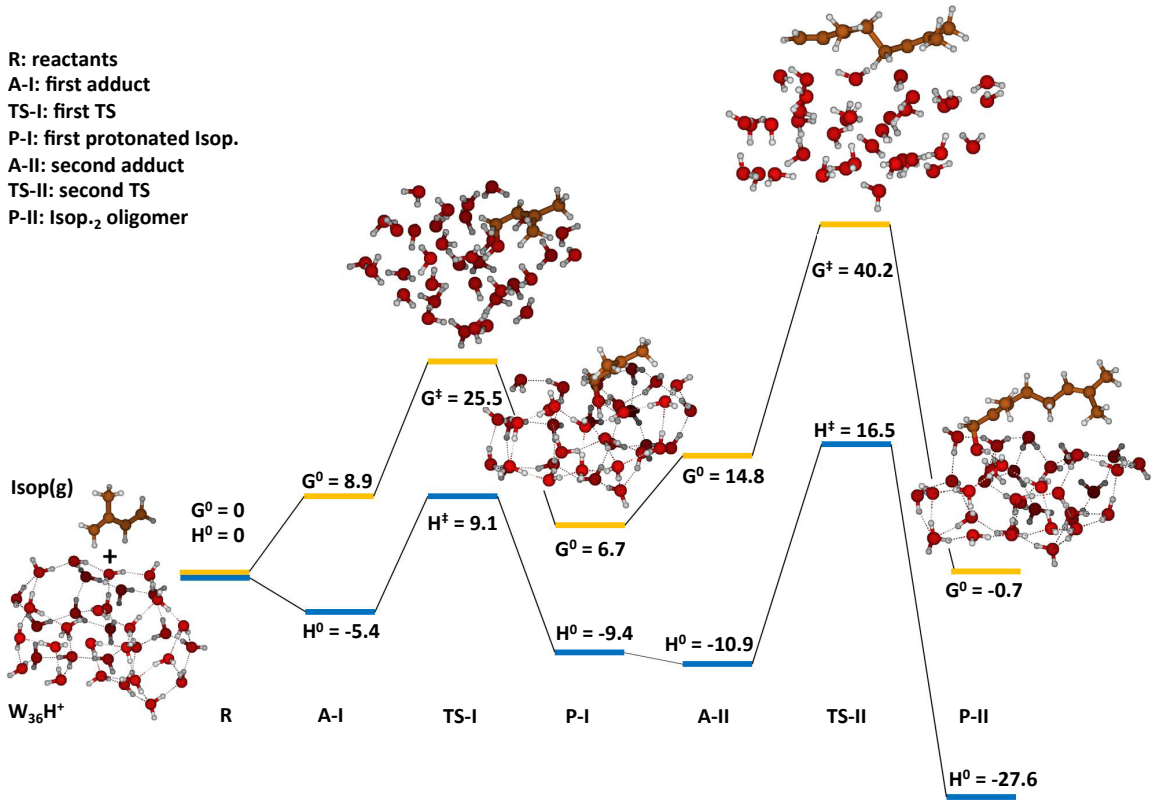

Figure A 1. Free energy and enthalpy landscapes for protonation and oligomerization of isoprene on a $(H_2O)_{36}H^+$ cluster representative of the mildly acidic surface of water. Given the small size of the cluster, the counter-ion was ignored. The kinetic barriers preventing proton transfer to isoprene and its subsequent oligomerization were $\Delta G^‡$ = 25.5 kcal mol^{-1} and $\Delta G^‡$ = 40.2 kcal mol^{-1}, respectively, which were insurmountable under ambient NTP conditions within a 1 ms timescale. (Image used with permission of the author(83)).

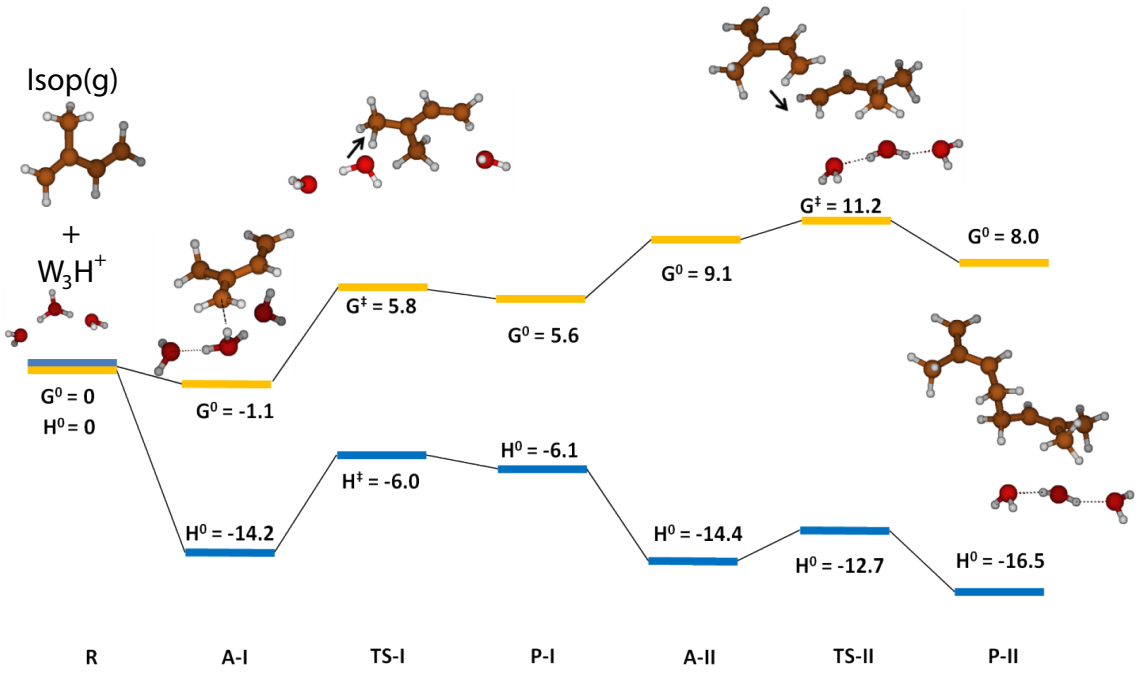

Figure A 2. Simulation of hydronium (G) with a small clusters of water produced during the ESIMS processes, $(H_2O)_3H^+$. Since the proton was insufficiently hydrated in this cluster, it exhibited extreme acidity: the incipient isoprene molecule (*Isop*) fell into a shallow potential well forming an adduct. The free energy barrier to proton transfer from $(H_2O)_3H^+$ to *Isop*(g) was $\Delta G^{\ddagger}$ = 6.9 kcal mol^{-1}; the barrier to subsequent oligomerization with another free *Isop*(g) was $\Delta G^{\ddagger}$ = 2.1 kcal mol^{-1}. Thus, it makes this a possible and likely reaction. (Image used with permission of the author(83)).

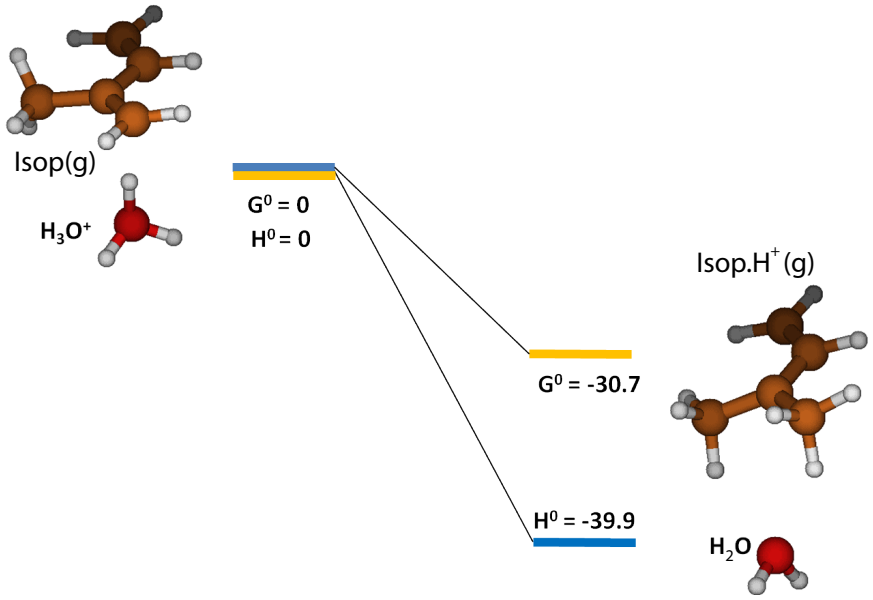

Figure A 3. *Ab initio* predictions of the proton transfer reaction between a gas-phase hydronium ion, H_3O^+(g), and a gas-phase isoprene molecule, *Isop*(g). Theory predicted the reaction to be spontaneous with a free energy change of ΔG^0 = - 30 kcal mol^{-1}, in accordance with the experimental gas-phase basicities (GB) of H_2O (GB_{H2O} = 157.7 kcal mol^{-1}) and *Isop* (GB_{ISO} = 190.6 kcal mol^{-1}); ΔGB = 32.9 kcal mol^{-1}. (Image used with permission of the author(83)).

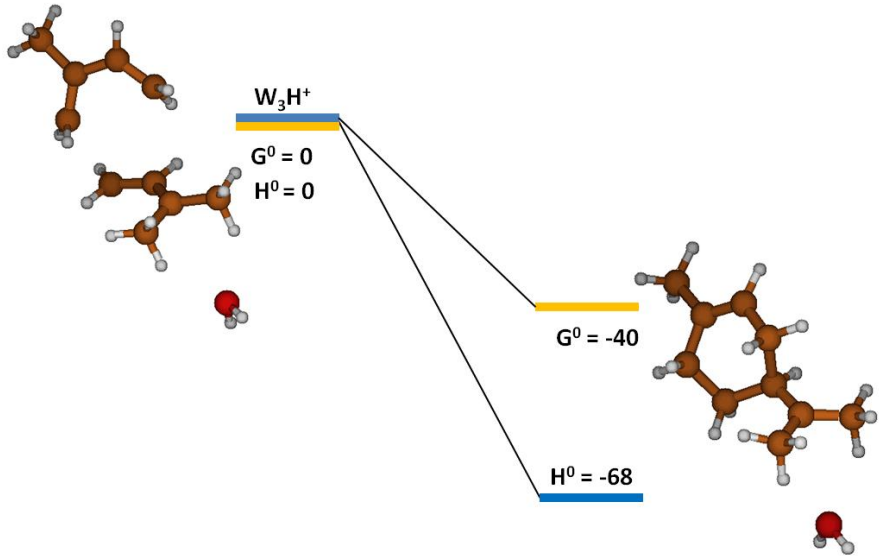

Figure A 4. Spontaneous gas-phase oligomerization of gas-phase cis-isoprene (*Isop*(g)) with a protonated trans-isoprene molecule, leading to a cyclic product. The units for G^0 and H^0 are kcal-mol^{-1}. (Image used with permission of the author(83)).

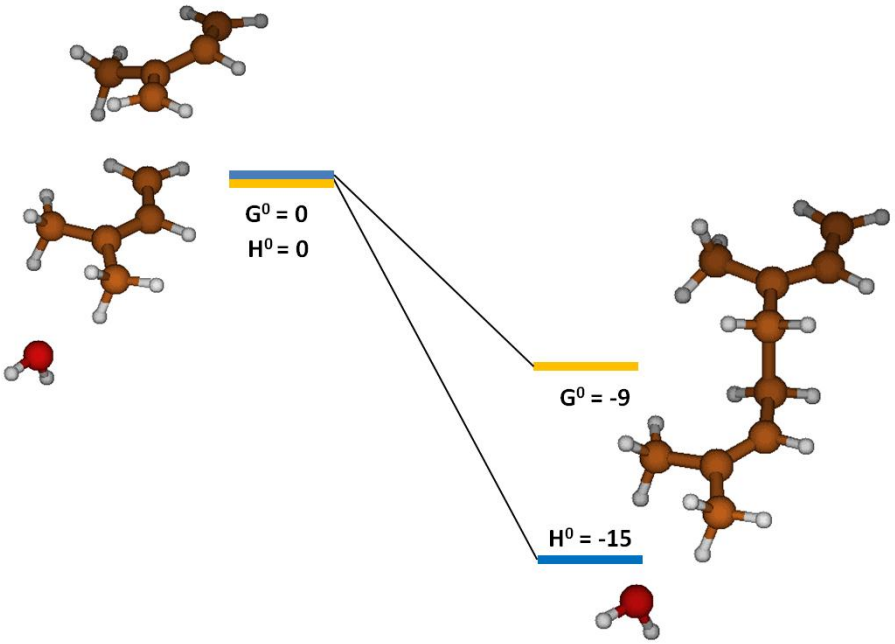

Figure A 5. Spontaneous gas-phase oligomerization of a trans-isoprene (*Isop*(g)) molecule with a protonated trans-isoprene, leading to a linear product. The units for G^0 and H^0 are kcal-mol^{-1}. (Image used with permission of the author(83)).

REFERENCE LIST

1. Cheng L, Fenter P, Nagy K, Schlegel M, & Sturchio N (2001) Molecular-scale density oscillations in water adjacent to a mica surface. *Physical Review Letters* 87(15):156103.

2. Lum K, Chandler D, & Weeks JD (1999) Hydrophobicity at small and large length scales. (ACS Publications).

3. Patel AJ, *et al*. (2011) Extended surfaces modulate hydrophobic interactions of neighboring solutes. *Proceedings of the National Academy of Sciences* 108(43):17678-17683.

4. Auer B & Skinner J (2009) Water: Hydrogen bonding and vibrational spectroscopy, in the bulk liquid and at the liquid/vapor interface. *Chemical physics letters* 470(1):13-20.

5. Martin G, Johnson D, & Spice A (1994) The measurement and parameterization of effective radius of droplets in warm stratocumulus clouds. *Journal of the Atmospheric Sciences* 51(13):1823-1842.

6. Kelley CP, Mohtadi S, Cane MA, Seager R, & Kushnir Y (2015) Climate change in the Fertile Crescent and implications of the recent Syrian drought. *Proceedings of the National Academy of Sciences* 112(11):3241-3246.

7. Chyba C & Sagan C (1992) Endogenous production, exogenous delivery and impact-shock synthesis of organic molecules: an inventory for the origins of life. *Nature* 355(6356):125-132.

8. Busschaert N & Gale PA (2013) Small‐Molecule Lipid‐Bilayer Anion Transporters for Biological Applications. *Angewandte Chemie International Edition* 52(5):1374-1382.

9. Brodhun F & Tittmann K (2015) Membrane enzymes: Transformers at the interface. *Nature chemical biology* 11(2):102-103.

10. Giorgio V, *et al*. (2013) Dimers of mitochondrial ATP synthase form the permeability transition pore. *Proceedings of the National Academy of Sciences* 110(15):5887-5892.

11. Zhao C-X (2013) Multiphase flow microfluidics for the production of single or multiple emulsions for drug delivery. *Advanced drug delivery reviews* 65(11):1420-1446.

12. Yu S, Wang X, & Wu D (2014) Microencapsulation of n-octadecane phase change material with calcium carbonate shell for enhancement of thermal

conductivity and serving durability: synthesis, microstructure, and performance evaluation. *Applied Energy* 114:632-643.

13. Huang H, *et al*. (2015) Emulsion synthesis of size-tunable CH3NH3PbBr3 quantum dots: an alternative route toward efficient light-emitting diodes. *ACS applied materials & interfaces* 7(51):28128-28133.

14. Yukuyama M, Ghisleni D, Pinto T, & Bou‐Chacra N (2016) Nanoemulsion: process selection and application in cosmetics‐a review. *International journal of cosmetic science* 38(1):13-24.

15. Galus S & Kadzińska J (2015) Food applications of emulsion-based edible films and coatings. *Trends in Food Science & Technology* 45(2):273-283.

16. Khan MKI, Maan AA, Schutyser M, Schroën K, & Boom R (2013) Electrospraying of water in oil emulsions for thin film coating. *Journal of Food Engineering* 119(4):776-780.

17. Cai W, *et al*. (2014) Increasing frequency of extreme El Niño events due to greenhouse warming. *Nature climate change* 4(2):111-116.

18. Tian CS & Shen YR (2009) Structure and charging of hydrophobic material/water interfaces studied by phase-sensitive sum-frequency vibrational spectroscopy. *Proc. Natl. Acad. Sci. U. S. A.* 106(36):15148-15153.

19. Thomas LL, Tirado-Rives J, & Jorgensen WL (2010) Quantum Mechanical/Molecular Mechanical Modeling Finds Diels-Alder Reactions Are Accelerated Less on the Surface of Water Than in Water. *J Am Chem Soc* 132(9):3097-3104.

20. Beattie JK, McErlean CSP, & Phippen CBW (2010) The Mechanism of On-Water Catalysis. *Chem-Eur J* 16(30):8972-8974.

21. Creux P, Lachaise J, Graciaa A, Beattie JK, & Djerdjev AM (2009) Strong Specific Hydroxide Ion Binding at the Pristine Oil/Water and Air/Water Interfaces. *J. Phys. Chem. B* 113(43):14146-14150.

22. Butler RN & Coyne AG (2016) Organic synthesis reactions on-water at the organic–liquid water interface. *Organic & biomolecular chemistry* 14(42):9945-9960.

23. Butler RN & Coyne AG (2015) Understanding "On-Water" Catalysis of Organic Reactions. Effects of H+ and Li+ Ions in the Aqueous Phase and Nonreacting Competitor H-Bond Acceptors in the Organic Phase: On H2O versus on D2O for Huisgen Cycloadditions. *The Journal of Organic Chemistry* 80(3):1809-1817.

24. Zhang C, *et al*. (2012) Water at hydrophobic interfaces delays proton surface-to-bulk transfer and provides a pathway for lateral proton diffusion. *Proceedings of the National Academy of Sciences* 109(25):9744-9749.

25. Harvey AH (1996) Semiempirical correlation for Henry's constants over large temperature ranges. *AIChE journal* 42(5):1491-1494.

26. Abraham MH, Whiting GS, Fuchs R, & Chambers EJ (1990) Thermodynamics of solute transfer from water to hexadecane. *Journal of the Chemical Society, Perkin Transactions 2* (2):291-300.

27. Patankar NA (2003) On the modeling of hydrophobic contact angles on rough surfaces. *Langmuir* 19(4):1249-1253.

28. Israelachvili JN (2011) *Intermolecular and surface forces* (Academic press).

29. Parker AR & Lawrence CR (2001) Water capture by a desert beetle. *Nature* 414(6859):33-34.

30. Du M, Zhao Y, Tian Y, Li K, & Jiang L (2016) Electrospun Multiscale Structured Membrane for Efficient Water Collection and Directional Transport. *Small* 12(8):1000-1005.

31. Hu DL, Chan B, & Bush JWM (2003) The hydrodynamics of water strider locomotion. *Nature* 424(6949):663-666.

32. Barthlott W & Neinhuis C (1997) Purity of the sacred lotus, or escape from contamination in biological surfaces. *Planta* 202(1):1-8.

33. Liu KS, Yao X, & Jiang L (2010) Recent developments in bio-inspired special wettability. *Chem Soc Rev* 39(8):3240-3255 (and references therein).

34. Freire E, Mayorga OL, & Straume M (1990) Isothermal titration calorimetry. *Analytical chemistry* 62(18):950A-959A.

35. Heinz WF & Hoh JH (1999) Spatially resolved force spectroscopy of biological surfaces using the atomic force microscope. *Trends in biotechnology* 17(4):143-150.

36. Kabza KG, Gestwicki JE, & McGrath JL (2000) Contact angle goniometry as a tool for surface tension measurements of solids, using Zisman plot method. A physical chemistry experiment. *J. Chem. Educ* 77(1):63.

37. Hammer MU, Anderson TH, Chaimovich A, Shell MS, & Israelachvili J (2010) The search for the hydrophobic force law. *Faraday discussions* 146:299-308.

38. Narayan S, *et al*. (2005) "On water": Unique reactivity of organic compounds in aqueous suspension. *Angew. Chem. Int. Ed.* 44(21):3275-3279.

39. Breslow R (1991) Hydrophobic Effects on Simple Organic-Reactions in Water. *Accounts Chem Res* 24(6):159-164.

40. Ingram AJ, Boeser CL, & Zare RN (2016) Going beyond electrospray: mass spectrometric studies of chemical reactions in and on liquids. *Chemical Science* 7(1):39-55.

41. Lee JK, Banerjee S, Nam HG, & Zare RN (2015) Acceleration of reaction in charged microdroplets. *Quarterly reviews of biophysics* 48(04):437-444.

42. Yan X, Bain RM, & Cooks RG (2016) Organic Reactions in Microdroplets: Reaction Acceleration Revealed by Mass Spectrometry. *Angew Chem Int Edit* 55(42):12960-12972.

43. Pulliam CJ, *et al*. (2017) Simultaneous Online Monitoring of Multiple Reactions Using a Miniature Mass Spectrometer. *Anal Chem* 89(13):6969-6975.

44. Jung YS & Marcus RA (2007) On the theory of organic catalysis on water. *J. Am. Chem. Soc.* 129(17):5492-5502.

45. Jung YS & Marcus RA (2010) Protruding interfacial OH groups and 'on-water' heterogeneous catalysis. *J Phys-Condens Mat* 22(28).

46. Hauner IM, Deblais A, Beattie JK, Kellay H, & Bonn D (2017) The Dynamic Surface Tension of Water. *Journal of Physical Chemistry Letters* 8(7):1599-1603.

47. Enami S, Hoffmann AR, & Colussi AJ (2008) Ozonolysis of uric acid at the air/water interface. *J. Phys. Chem. B* 112(14):4153-4156.

48. Enami S, Hoffmann MR, & Colussi AJ (2008) Acidity enhances the formation of a persistent ozonide at aqueous ascorbate/ozone gas interfaces. *Proc. Acad. Natl. Sci. U.S.A.* 105(21):7365-7369.

49. Enami S, Hoffmann MR, & Colussi AJ (2008) Ozonolysis of uric acid at the air/water interface. *J. Phys. Chem. B* 112(14):4153-4156.

50. Enami S, Hoffmann MR, & Colussi AJ (2009) How phenol and alpha-tocopherol react with ambient ozone at gas/liquid interfaces. *J. Phys. Chem. A* 113(25):7002-7010.

51. Enami S, Hoffmann MR, & Colussi AJ (2009) Simultaneous detection of cysteine sulfenate, sulfinate, and sulfonate during cysteine interfacial ozonolysis. *J. Phys. Chem. B* 113(28):9356-9358.

52. Enami S, Hoffmann MR, & Colussi AJ (2009) Absorption of Inhaled NO2. *J. Phys. Chem. B* 113(23):7977-7981.

53. Enami S, Hoffmann MR, & Colussi AJ (2009) Ozone Oxidizes Glutathione to a Sulfonic Acid. *Chem. Res. Toxicol.* 22(1):35-40.

54. Enami S, Hoffmann MR, & Colussi AJ (2010) Prompt Formation of Organic Acids in Pulse Ozonation of Terpenes on Aqueous Surfaces. *J. Phys. Chem. Lett.* 1(15):2374-2379.

55. Enami S, Hoffmann MR, & Colussi AJ (2010) Proton Availability at the Air/Water Interface. *J. Phys. Chem. Lett.* 1(10):1599-1604.

56. Enami S, Hoffmann MR, & Colussi AJ (2010) Molecular Control of Reactive Gas Uptake "on Water". *J. Phys. Chem. A* 114(18):5817-5822.

57. Enami S, Hoffmann MR, & Colussi AJ (2010) Superacid chemistry on mildly acidic water. *J. Phys. Chem. Lett.* 1(24):3488-3493.

58. Enami S, Hoffmann MR, & Colussi AJ (2012) Dry deposition of biogenic terpenes via cationic oligomerization on environmental aqueous surfaces *J. Phys. Chem. Lett.* 3 3102-3108.

59. Enami S, Mishra H, Hoffmann MR, & Colussi AJ (2012) Protonation and Oligomerization of Gaseous Isoprene on Mildly Acidic Surfaces: Implications for Atmospheric Chemistry. *J Phys Chem A* 116(24):6027-6032.

60. Enami S, Vecitis CD, Cheng J, Hoffmann MR, & Colussi AJ (2008) Mass spectrometry of interfacial layers during fast aqueous aerosol/ozone gas reactions of atmospheric interest. *Chem. Phys. Lett.* 455(4-6):316-320.

61. Hayase S, *et al*. (2010) Heterogeneous Reaction of Gaseous Ozone with Aqueous Iodide in the Presence of Aqueous Organic Species. *J. Phys. Chem. A* 114(19):6016-6021.

62. Mishra H, *et al*. (2012) Anions dramatically enhance proton transfer through aqueous interfaces. *Proc. Acad. Natl. Sci. U.S.A.* 109(26):10228-10232.

63. Mishra H, *et al*. (2012) Bronsted basicity of the air-water interface *Proc. Acad. Natl. Sci. U.S.A.*:doi/10.1073/pnas.1209307109.

64. Yabushita A, *et al*. (2009) Anion-Catalyzed Dissolution of NO_2 on Aqueous Microdroplets. *J. Phys. Chem. A* 113(17):4844-4848.

65. Wu C, Siems WF, & Hill HH (2000) Secondary electrospray ionization ion mobility spectrometry/mass spectrometry of illicit drugs. *Analytical chemistry* 72(2):396-403.

66. Huang M-Z, Yuan C-H, Cheng S-C, Cho Y-T, & Shiea J (2010) Ambient ionization mass spectrometry. *Annual review of analytical chemistry* 3:43-65.

67. Martinez-Lozano P, Rus J, de la Mora GF, Hernandez M, & de la Mora JF (2009) Secondary Electrospray Ionization (SESI) of Ambient Vapors for Explosive Detection at Concentrations Below Parts Per Trillion. *Journal of the American Society for Mass Spectrometry* 20(2):287-294.

68. Thomas DA, Wang LT, Goh B, Kim ES, & Beauchamp JL (2015) Mass Spectrometric Sampling of a Liquid Surface by Nanoliter Droplet Generation from Bursting Bubbles and Focused Acoustic Pulses: Application to Studies of Interfacial Chemistry. *Anal Chem* 87(6):3336-3344.

69. Kazansky VB (2002) Solvation as a main factor that determines the strength of liquid superacids and the selectivity of the acid-catalyzed reactions of olefins. *Catalysis Today* 73(1-2):127-137.

70. Kauzmann W (1959) Some Factors in the Interpretation of Protein Denaturation. *Adv Protein Chem* 14:1-63.

71. Adair Gallo Junior, Andreia S. Farinha, Miguel Dinis, Abdul-Hamid Emwas, Robert J. Nielsen, William A. Goddard III, Himanshu Mishra (2018) Could Electrospray Ionization Mass Spectrometry Investigate Ambient Chemical Reactions at the Air-Water Interface in Real Time? *Under review*.

72. Bain RM, Pulliam CJ, & Cooks RG (2015) Accelerated Hantzsch electrospray synthesis with temporal control of reaction intermediates. *Chemical Science* 6(1):397-401.

73. De Hoffmann E & Stroobant V (2007) *Mass spectrometry: principles and applications* (John Wiley & Sons).

74. Banerjee S & Mazumdar S (2012) Electrospray Ionization Mass Spectrometry: A Technique to Access the Information beyond the Molecular Weight of the Analyte. *International Journal of Analytical Chemistry*.

75. Kebarle P & Verkerk UH (2009) Electrospray: From Ions in Solution to Ions in the Gas Phase, What We Know Now. *Mass Spectrometry Reviews* 28(6):898-917.

76. Tabe Y, Kikkawa N, Takahashi H, & Morita A (2013) Surface Acidity of Water Probed by Free Energy Calculation for Trimethylamine Protonation. *The Journal of Physical Chemistry C* 118(2):977-988.

77. Colussi AJ & Enami S (2014) Comment on "Surface Acidity of Water Probed by Free Energy Calculation for Trimethylamine Protonation". *The Journal of Physical Chemistry C* 118(5):2894-2894.

78. Wortmann A, *et al*. (2007) Shrinking droplets in electrospray ionization and their influence on chemical equilibria. *J Am Soc Mass Spectr* 18(3):385-393.

79. Mora JFdl, *et al*. (2000) Electrochemical processes in electrospray ionization mass spectrometry. *Journal of Mass Spectrometry* 35(8):939-952.

80. Muller T, Badu-Tawiah A, & Cooks RG (2012) Accelerated Carbon-Carbon Bond-Forming Reactions in Preparative Electrospray. *Angew Chem Int Edit* 51(47):11832-11835.

81. Zhou SL & Cook KD (2000) Protonation in electrospray mass spectrometry: Wrong-way-round or right-way-round? *J Am Soc Mass Spectr* 11(11):961-966.

82. Banerjee S, Prakash H, & Mazumdar S (2011) Evidence of Molecular Fragmentation inside the Charged Droplets Produced by Electrospray Process. *J Am Soc Mass Spectr* 22(10):1707-1717.

83. Mishra H (2013) Proton transfers at the air-water interface. (Dissertation (Ph.D.), California Institute of Technology).

84. Ball P (2008) Water as an active constituent in cell biology. *Chemical reviews* 108(1):74-108.

85. Ball P (2008) Water as a biomolecule. *ChemPhysChem* 9(18):2677-2685.

86. Ball P (2011) Biophysics: More than a bystander. *Nature* 478(7370):467-468.

87. Chaplin M (Water Structure and Science.

88. Fenn JB (2003) Electrospray wings for molecular elephants (Nobel lecture). *Angew Chem Int Edit* 42(33):3871-3894.

89. Eberlin MN (2007) Electrospray ionization mass spectrometry: a major tool to investigate reaction mechanisms in both solution and the gas phase. *European Journal of Mass Spectrometry* 13(1):19-28.

90. Yamashita M & Fenn JB (1984) Electrospray ion-source - another variation on the free-jet theme. *J. Phys. Chem.* 88(20):4451-4459.

91. de la Mora JF (2007) The fluid dynamics of Taylor cones. *Annu Rev Fluid Mech* 39:217-243.

92. Luedtke WD, *et al*. (2008) Nanojets, electrospray, and ion field evaporation: Molecular dynamics simulations and laboratory experiments. *Journal of Physical Chemistry A* 112(40):9628-9649.

93. Collins RT, Jones JJ, Harris MT, & Basaran OA (2008) Electrohydrodynamic tip streaming and emission of charged drops from liquid cones. *Nature Physics* 4(2):149-154.

94. Rayleigh L (1882) XX. On the equilibrium of liquid conducting masses charged with electricity. *The London, Edinburgh, and Dublin Philosophical Magazine and Journal of Science* 14(87):184-186.

95. Kebarle P & Peschke M (2000) On the mechanisms by which the charged droplets produced by electrospray lead to gas phase ions. *Anal. Chim. Acta* 406(1):11-35.

96. Moseler M & Landman U (2000) Formation, stability, and breakup of nanojets. *Science* 289(5482):1165-1169.

97. Nguyen S & Fenn JB (2007) Gas-phase ions of solute species from charged droplets of solutions. *Proc. Natl. Acad. Sci. U. S. A.* 104(4):1111-1117.

98. Sharkey TD, Wiberley AE, & Donohue AR (2008) Isoprene emission from plants: Why and how. *Annals of Botany* 101(1):5-18.

99. Hurst JM, *et al.* (2001) Investigation of the nighttime decay of isoprene. *J Geophys Res-Atmos* 106(D20):12.

100. Barkley MP, *et al.* (2008) Net ecosystem fluxes of isoprene over tropical South America inferred from Global Ozone Monitoring Experiment (GOME) observations of HCHO columns. *J Geophys Res-Atmos* 113(D20).

101. Guenther A, *et al.* (2006) Estimates of global terrestrial isoprene emissions using MEGAN (Model of Emissions of Gases and Aerosols from Nature). *Atmos. Chem. Phys.* 6:3181-3210.

102. Archibald AT, *et al.* (2011) Impacts of HO(x) regeneration and recycling in the oxidation of isoprene: Consequences for the composition of past, present and future atmospheres. *Geophys Res Lett* 38(L05804):6.

103. Di Carlo P, *et al.* (2004) Missing OH reactivity in a forest: Evidence for unknown reactive biogenic VOCs. *Science* 304(5671):722-725.

104. Yokouchi Y & Ambe Y (1988) Diurnal variations of atmospheric isoprene and monoterpene hydrocarbons in an agricultural area in summertime. *Journal of Geophysical Research: Atmospheres* 93(D4):3751-3759.

105. Anonymous (2017) National Center for Biotechnology Information. in *PubChem Compound Database: CID=6557*.

106. Spence TG, Burns TD, & Posey LA (1997) Controlled Synthesis of Transition-Metal Ion Complex/Solvent Clusters by Electrospray Ionization. *The Journal of Physical Chemistry A* 101(2):139-144.

107. Van Berkel GJ, McLuckey SA, & Glish GL (1992) Electrochemical origin of radical cations observed in electrospray ionization mass spectra. *Analytical Chemistry* 64(14):1586-1593.

108. Aussillous P & Quere D (2001) Liquid marbles. *Nature* 411(6840):924-927.

109. Smith JN, Flagan RC, & Beauchamp JL (2002) Droplet evaporation and discharge dynamics in electrospray ionization. *J Phys Chem A* 106(42):9957-9967.

110. Zhou S, Prebyl BS, & Cook KD (2002) Profiling pH changes in the electrospray plume. *Analytical chemistry* 74(19):4885-4888.

111. Schroder D, Budesinsky M, & Roithova J (2012) Deprotonation of p-Hydroxybenzoic Acid: Does Electrospray Ionization Sample Solution or Gas-Phase Structures? *Journal of the American Chemical Society* 134(38):15897-15905.

112. Schroder D (2012) Ion clustering in electrospray mass spectrometry of brine and other electrolyte solutions. *Physical Chemistry Chemical Physics* 14(18):6382-6390.

113. Bain RM, Pulliam CJ, Thery F, & Cooks RG (2016) Accelerated Chemical Reactions and Organic Synthesis in Leidenfrost Droplets. *Angew Chem Int Edit* 55(35):10478-10482.

114. Donaldson DJ & Valsaraj KT (2010) Adsorption and Reaction of Trace Gas-Phase Organic Compounds on Atmospheric Water Film Surfaces: A Critical Review. *Environ. Sci. Technol.* 44(3):865-873.

115. Blake RS, Monks PS, & Ellis AM (2009) Proton-Transfer Reaction Mass Spectrometry. *Chemical Reviews* 109(3):861-896.

116. Wei Z, Wleklinski M, Ferreira C, & Cooks RG (2017) Reaction Acceleration in Thin Films with Continuous Product Deposition for Organic Synthesis. *Angewandte Chemie International Edition* 56(32):9386-9390.

117. Bryantsev VS, Diallo MS, & Goddard WA (2009) Computational Study of Copper(II) Complexation and Hydrolysis in Aqueous Solutions Using Mixed Cluster/Continuum Models. *Journal of Physical Chemistry A* 113(34):9559-9567.

118. Sarotti AM, Suarez AG, & Spanevello RA (2011) DFT calculations induced a regiochemical outcome revision of the Diels-Alder reaction between levoglucosenone and isoprene. *Tetrahedron Lett.* 52(24):3116-3119.

119. Zhao Y & Truhlar DG (2008) The M06 suite of density functionals for main group thermochemistry, thermochemical kinetics, noncovalent interactions, excited states, and transition elements: two new functionals and systematic testing

of four M06-class functionals and 12 other functionals. *Theor Chem Acc* 120(1-3):215-241.

120. Kelly CP, Cramer CJ, & Truhlar DG (2004) Predicting Adsorption Coefficients at Air-Water Interfaces Using Universal Solvation and Surface Area Models. *J. Phys. Chem. B* 108:12882-12897.

121. Clark T, Chandrasekhar J, Spitznagel GW, & Schleyer PV (1983) Efficient Diffuse Function-Augmented Basis Sets for Anion Calculations. Iii. The 3-21+G Basis Set for First-Row Elements, Li-F. *J Comput Chem* 4(3):8.

122. Hunter EPL & Lias SG (1998) Evaluated gas phase basicities and proton affinities of molecules: An update. *J. Phys. Chem. Ref. Data* 27(3):413-656.

123. Kazansky VB (2001) Solvation effects in catalytic transformations of olefins in sulfuric acid. *Catal. Rev.* 43(3):199-232.